A Generalisable Stiffness Metric for Joint Configuration Optimisation of Serial Manipulators

Thesis – Master Robotics

Thomas Hettasch

2025-04-25

TU Delft supervisor	Martijn Wisse	M.Wisse@tudelft.nl
Company supervisor	Aashish Vatsyayan	A.Vatsyayan@tudelft.nl
Company supervisor	Eugenio Bernardi	E.Bernardi@tudelft.nl

Dedication

To my grandfather, Albrecht Kistner,
Who studied in Delft before me
And instilled within me
An undying curiosity
For the workings of our world

A Generalisable Stiffness Metric for Joint Configuration Optimisation of Serial Manipulators

Thomas Hettasch

Abstract—There is growing demand for use of serial robotic manipulators in machining, as they are more flexible and affordable than conventional CNC machines. Maintaining positional accuracy under load is crucial to ensure adequate process performance. Offline, configuration-based stiffness optimisation can be used to achieve improved stiffness characteristics for a given process. A new stiffness metric is proposed, which aims to predict how well a process will adhere to its positional tolerances under load for a given joint-configuration. The proposed metric is validated for through-drilling using a Kuka LBR iiwa 14 R820 cobot. It is shown that the metric correlates with the lateral controller tracking error (Spearman's rank correlation coefficient of 0.93) and the hole diameter (0.81). The correlations are better than those of existing metrics. The controller error can be decreased from a worst case of $380\,\mu\mathrm{m}$ down to $68\,\mu\mathrm{m}$, a reduction of more than a factor of 5. A flexible software framework for performing these optimisations is also made available.

1 Introduction

Serial robotic manipulators are ubiquitous in the field of automation and are widely used for tasks without significant contact loads (e.g. painting). Due to their low cost and high flexibility, there is growing demand for using these manipulators in more demanding applications, where loads and accuracy requirements are higher [1]. The field of interest here is robotic machining, i.e. use of robots in machining processes such as drilling, milling or grinding.

For example, during aircraft manufacturing, it is still occasionally necessary for manual drilling to be performed. Due to the scale and curvature of fuselage parts, traditional computer numerical control (CNC) solutions, such as 3 axis-mills, cannot be used. The added flexibility and reach of a serial manipulator could possibly enable automation of the drilling process.

A key reason why serial manipulators have not seen much use in robotic machining, is their lack of accuracy, particularly when compared to traditional CNC solutions. A dominant source of this error is the deflection of the manipulator under load [2]. For this reason, many researchers have looked into improving the stiffness characteristics of serial robots and thus the accuracy of the process [3]–[8].

Generally, these solutions depend on proprietary software [3], [4], [8]–[10]. Many common machining processes have been studied, including milling [4], [6], [9], [11]–[14], grinding/polishing [14]–[18], drilling [5], [19], deburring [20] and welding [21]. Each is approached separately and no generic methodology is available.

The underlying premise used to improve a robot's stiffness behaviour lies in recognising that different joint configurations of the robot yield different Cartesian stiffness. Thus, by leveraging redundant degrees of freedom, improved stiffness characteristics may be identified. Since the procedure does not rely on force or torque sensors, it is applicable to both industrial and collaborative robots (cobots).

Different metrics[a] may be used in optimising the stiffness characteristics, however existing options are either highly generic or overly restrictive. This report proposes a new metric, which may be used to optimise stiffness for a process, given its tolerances. The solution is implemented in a flexible software framework to allow for further development and use of the metric.

Section 2 outlines how the robot's stiffness is modelled. Stiffness metrics, including the newly proposed tolerance metric, are discussed in Section 3. Then, an overview over the software framework is provided in Section 4. Next, the metric is experimentally verified. First, the joint stiffnesses are determined (Section 5), then the metric is applied in a robotic drilling application (Section 6). Finally, the results of the experimental work are discussed and the applicability of the developed metric assessed (Section 7).

2 Theory: Robot Model

To improve the stiffness of a robotic manipulator with the aim of improving process accuracy, the stiffness behaviour at the end-effector must be modelled. If a force (or more generally, a wrench) is applied at the end-effector, there may be some deflection of the end-effector. The Cartesian stiffness defines the relationship between the wrench and the deflection, and is affected by multiple factors.

Some of the deflection is mechanical in nature. The links comprising the robot, the joints connecting the links, the base of the robot and the end-effector itself are all susceptible to

a. The term metric is conceptually equivalent to a cost, evaluation or reward function (with alterations to the sign where necessary) deformation. Additionally, there may be deflection due to corrections from the motor controllers, which have to compensate for changes in loading, thus temporarily producing unwanted deflection from the nominal pose.

It may be possible to model each effect in great detail, for example by creating finite element models of the links, or analysing the motor's control systems in depth. In practice, relatively simple models are often used, as these have fewer parameters and are thus more practical to use (see Section 2.2).

2.1 Generic Model

A stiffness model relates the Cartesian displacement δX and applied wrench F at the end-effector of a robot. These 6-dimensional vectors encode both the linear/translational and angular/rotational components. Appendix A contains a more complete description, including formulations for transforming displacements and twists between coordinate frames.

A linear model can be expressed as follows, where K_x is a 6×6 matrix encoding the stiffness of the system. Often, it is convenient to use the inverse of the stiffness matrix, i.e. the Cartesian compliance matrix C_x. These matrices must be positive semi-definite.

$$F = K_x \delta X \tag{2.1}$$

$$\delta X = C_x F \tag{2.2}$$

2.2 Virtual Joint Model

One means of computing the compliance matrix often used in stiffness analysis of serial manipulators is the Virtual Joint Modelling (VJM) method [3]–[5], [7], [11], [12], [14], [15], [19], [22], [23]. It was first developed by Salisbury [24] and later refined by Alici and Shirinzadeh [25]. Only the joint compliances are taken into account. The significantly stiffer links [26] are not considered.

For the simplified model [24], the Cartesian stiffness K_x at the end-effector is:

$$K_x = J^{-T} K_q J^{-1} \tag{2.3}$$

Where J is the robot Jacobian[b] and K_q is a diagonal matrix of the joint stiffnesses.

Since the inverse operation may be time consuming to compute, an inverse of the stiffness matrix is sometimes used instead, namely, the compliance matrix (C_x) [11]. The diagonal joint stiffness matrix is replaced by the diagonal joint compliance matrix C_q. This formulation is especially useful for over- and under-actuated manipulators, since their non-square Jacobians are not conventionally invertible. A derivation of this model is provided in Appendix B.

$$K_x^{-1} = C_x = J C_q J^T \tag{2.4}$$

This leads to a final expression for predicted robot deflection of:

$$\delta X = J C_q J^T F \tag{2.5}$$

b. Note that J^{-T} represents the inverse of the transpose of the robot Jacobian J

Note that the deflection and the wrench must be represented in the robot's base frame. The point at which the deflection is measured is the tip of the kinematic chain (as expressed by the Jacobian). The same is true for the point the wrench is applied at. In some cases, an expression in a different frame or at a different point may have to be considered. This may be achieved using specialised transformation matrices, which are derived in Appendix A.

The focus of this report lies primarily on the stiffness metric, thus the suitability of more complex models is not explored in detail. Due to its use in previous research, it is accepted that the simplified VJM model is sufficient for stiffness optimisation and will be used throughout. Stiffness metrics are explored next, which quantify the suitability of certain stiffness behaviours.

3 Theory: Stiffness Metrics

In order to optimise the stiffness of a serial manipulator, some means of comparing the suitability of one configuration to another must be established. This metric may be considered as a cost or reward function. In configuration-based stiffness optimisation it takes the form $f(q)$. It is common for this function to be applied directly to the compliance matrix, in other words $f(q) = g(C_x(q))$.

An overview of existing metrics is given below. Note that most are either not parametrisable, or the relationship between the parameters and the expected machining performance is tenuous.

3.1 Existing Metrics

3.1.1 Eigenvectors and Eigenvalues

The Eigenvectors of the compliance matrix identify directions in which compliance is uncoupled [27]. In other words, a force acting along an Eigenvector of the compliance matrix will result in a deflection along the same vector. The compliance in this direction is given by the Eigenvalue. While this forms a useful tool for understanding the compliance behaviour, it does not directly offer a means of scoring or comparing the behaviour.

3.1.2 Isometry

By computing the ratio between the maximum and minimum Eigenvalues of the Cartesian stiffness matrix, a measure of stiffness isometry is obtained [28]–[30]. If this ratio is close to one, the stiffness behaviour is roughly uniform, i.e. the same in all directions. This metric does not take into account the actual stiffness, nor any directional information, thus it is not expected to be particularly useful for robotic machining applications.

3.1.3 Determinant

The determinant of the stiffness matrix has been used as a stiffness metric [5], [14], [31], however its physical relevance and mathematical rigour is lacking (the stiffness matrix is not dimensionally homogeneous).

3.1.4 Desired Stiffness Matrix

The actual stiffness matrix may be matched to a desired stiffness matrix by use of the Frobenius norm [32]–[34], however this may be overly restrictive in a scenario where there is only limited capacity to alter the stiffness behaviour. Additionally, there is the challenge of choosing a desired stiffness matrix in the first place.

3.1.5 Screw Stiffness

The stiffness along a specific screw (direction, having both a linear and angular component) may be found. This forms a useful metric, since it is often valuable to only focus on the stiffness in a process-relevant direction. However, this metric cannot account for cases where the applied wrench and unwanted deflection have different directions.

3.2 Tolerance Metric

In light of the shortcomings of existing metrics for scoring robot stiffness, a new metric was developed, which captures the requirements of a given process, allowing for it to be tailored to a specific process, while remaining general enough to be applicable to any process.

A key requirement common to all machining processes is adherence to geometric and dimensional tolerances. Tool deflection during machining and the machining errors are related, thus it would be reasonable to require the deflections (as predicted by the stiffness model) to fall within some tolerance bounds. Note that for comparing two cases, it would be useful to not just obtain a binary pass/fail result, but rather a value indicating how close a process is to falling within tolerance.

A simple, one-dimensional example is used to introduce the workings of the tolerance metric. Then a two-dimensional example is used to build on the concept. Finally, a generic formulation will be shown.

3.2.1 An Introductory Example

A deflection δx from a nominal pose may be required to fall between bounds of $+\epsilon$ and $-\epsilon$. This may be expressed as:

$$|\delta x| \leq \epsilon \tag{3.1}$$

This expression is equivalent to the following:

$$\delta x^2 \leq \epsilon^2 \tag{3.2}$$

$$\frac{\delta x^2}{\epsilon^2} \leq 1 \tag{3.3}$$

$$m = \sqrt{\frac{\delta x^2}{\epsilon^2}} \leq 1 \tag{3.4}$$

Note that the smaller the term m, the closer the deflection is to zero and is exactly at zero for $m = 0$. For a value of $m = 1$, the deflection is exactly at the tolerance bound. If m exceeds one, the deflection is not within tolerance.

3.2.2 Simple 2D Example

Consider a two dimensional case, where a vertical through hole is drilled (Figure 3.1). Neither the top, nor the bottom of the drillbit should veer more than some tolerance off its path laterally. Let this tolerance be represented by ϵ.

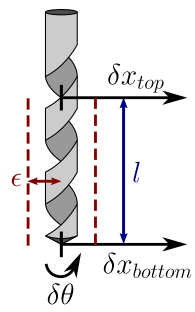

Fig. 3.1: Drilling tolerance example

Then:

$$|\delta x_{bottom}| = |\delta x| \leq \epsilon \tag{3.5}$$

$$\text{and} \quad |\delta x_{top}| = |\delta x - l\delta\theta| \leq \epsilon \tag{3.6}$$

Both these conditions must hold for the drill to be within tolerance. These conditions can be rewritten as:

$$\frac{\delta x^2}{\epsilon^2} \leq 1 \tag{3.7}$$

$$\frac{(\delta x - l\delta\theta)^2}{\epsilon^2} \leq 1 \tag{3.8}$$

If the following holds, both of the above conditions must necessarily hold too:

$$\frac{\delta x^2}{\epsilon^2} + \frac{(\delta x - l\delta\theta)^2}{\epsilon^2} \leq 1 \tag{3.9}$$

This combined tolerance can be rewritten in quadratic form as:

$$\begin{bmatrix} \delta x & \delta\theta \end{bmatrix} \begin{bmatrix} \frac{2}{\epsilon^2} & -\frac{l}{\epsilon^2} \\ -\frac{l}{\epsilon^2} & \frac{l^2}{\epsilon^2} \end{bmatrix} \begin{bmatrix} \delta x \\ \delta\theta \end{bmatrix} \leq 1 \tag{3.10}$$

This combined tolerance may be visualised as an ellipse (see Figure 3.2). Note that the tolerance bounds at the bottom of the drill are denoted by Limit A, and the top of the drill is denoted by Limit B. If a deflection is within the ellipse, it is within tolerance.

3.2.3 The Full Expression

This concept may be generalised to 6-dimensional vectors, i.e. full 6 degree of freedom deflections, as follows:

$$m = \sqrt{(\delta X^T)\,\mathcal{T}\,(\delta X)} \leq 1 \tag{3.11}$$

Where δX is the predicted Cartesian deflection, and $\mathcal{T}$ is a 6×6 matrix encoding the specific process requirement.

In this way, positional tolerances at a point, angular tolerances, as well as combinations of the two may be expressed. Appendix C contains more elaborate details. Two tolerances may be added through simple summation, resulting in a combined tolerance that is more conservative than either individual tolerance. Finally, the point at which the tolerance is applied can be chosen arbitrarily, allowing for a flexible, but compact means of expressing engineering tolerances.

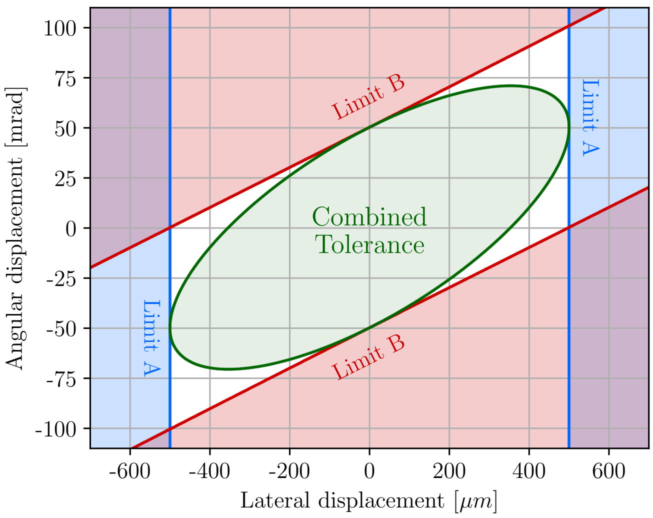

Fig. 3.2: 2D drilling tolerance visualisation ($\epsilon = 500\mu\text{m}$, $l = 10\text{mm}$)

3.2.4 Additional Considerations

The method also has some drawbacks, such as always being symmetrical around the nominal pose and becoming increasingly restrictive under the addition of multiple tolerances. Finally, it should be noted that this tolerance applies to the relative positioning of the end-effector and does not necessarily translate directly to the geometrical tolerances measured on a machined workpiece.

For this to be used as a stiffness metric, it is necessary to have some understanding of the wrench that is expected to be applied at the end-effector. This wrench is then passed through the stiffness model to obtain an expected deflection, which can then be compared to the tolerance as described above. Since the output is not purely binary, it may be used in a gradient based optimisation algorithm. The full computation is summarised in Figure 3.3.

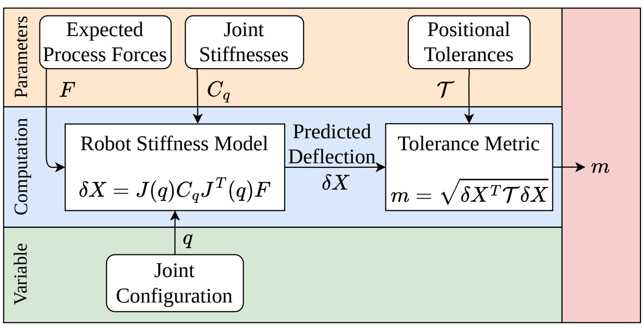

Fig. 3.3: Summary of metric computation

Note that any robot model $\delta X(F)$ may theoretically be used, however a linear model (such as the simplified VJM), is advantageous when dealing with uncertain process forces (see Section 3.3.2).

3.3 Dealing with Uncertainty

The exact process forces under contact are very difficult to predict and are affected by so many factors that exact prediction of the instantaneous process force is futile in a real world application. Two means of compensating for varying process forces are provided, one for variations that can be predicted and one for variations that cannot.

3.3.1 Known Variations

The process forces during machining may vary significantly due to many factors[c]. For example, the normal force experienced during drilling may change drastically with feed speed and tool wear. Some effects may be modelled using a multivariate normal distribution. Both the expected mean and variation of the expected process wrench may be represented. Couplings between directions can also be represented, namely as covariances. This allows for modelling of effects such as the changing axial moment due to changing normal forces.

While process wrenches may not be distributed normally, the multivariate normal is nevertheless a useful modelling tool, as it is closed under affine transformation. In other words, if a multivariate normal wrench is fed into a linear stiffness model, a multivariate normal deflection is returned. If said deflection is then passed through the proposed tolerance metric, a generalised chi-squared distribution is obtained. By computing either its cumulative distribution function (CDF) or expected value, the initial uncertainty of the wrench can be accounted for in the final metric.

3.3.2 Unknown Variations

There may be cases where the absolute applied force is not known and cannot be predicted with any amount of certainty. If a linear stiffness model is used (such as the VJM model used throughout this report), a rudimentary understanding of the process force's direction is sufficient for stiffness optimisation. In other words, if the wrench direction u_f is known, but its magnitude $\|F\|$ is not, the metric may be computed with the direction u_f. The metric $m_{absolute}$, computed using the wrench F, and the metric $m_{relative}$, computed using the wrench direction u_f, are linearly proportional:

$$F = \|F\|\, u_f \tag{3.12}$$

$$\delta X = C_x \,\|F\|\, u_f \tag{3.13}$$

$$m_{\text{absolute}} = \sqrt{u_f^T C_x^T \,\|F\|\; \mathcal{T}\; C_x \,\|F\|\, u_f} \tag{3.14}$$

$$m_{\text{absolute}} = \|F\| \sqrt{\left(u_f^T C_x^T \;\mathcal{T}\; C_x u_f\right)} \tag{3.15}$$

$$m_{\text{absolute}} = \|F\|\; m_{\text{relative}} \tag{3.16}$$

$$\text{therefore} \quad m_{\text{absolute}} \propto m_{\text{relative}} \tag{3.17}$$

Knowing that the optimisation procedure merely searches for an extremum of the stiffness metric, the relative tolerance metric ($m_{relative}$) can be used for optimisation. Thus it is sufficient to use the direction of the force for estimating the deflection. Absolute claims about tolerance adherence can no longer be made under these assumptions.

c. A full list is not relevant here, but may be required for detailed analysis of the process forces.

4 Software Framework

To study the efficacy of different stiffness metrics, as well as finding optimal robot joint configurations, a flexible software framework was developed and dubbed **reflex** (Flexible Robot Evaluation Framework[d]). While the key scientific novelty of this thesis is the tolerance stiffness metric, **reflex** will hopefully enable researchers and engineers from academia and industry to actually use stiffness optimisation and develop the field further. A detailed description of the architecture of **reflex** is available in Appendix G.

The **reflex** framework was developed to be as generic and modular as possible, allowing for simple binding to existing packages, such as *MoveIt2* [35] and *reach* [36]. The core of the framework does not depend on these external tools and extensibility is implemented using plugins. This opens the possibility of using the core functionality with different tools, such as *ROS(2)*, *RoboDK* or *Blender*.

Two applications of the framework are shown below, which were used in preparing the experiment described in Section 6.

4.1 Displacement Visualisation

To gain an understanding into how the robot is expected to displace under load, a visualisation pipeline was developed. Figure 4.1 shows a screenshot from this visualisation (note that the magnitude of the displacement is exaggerated for clarity). The displacement prediction is updated in real-time, responding to changes in the applied wrench or robot pose.

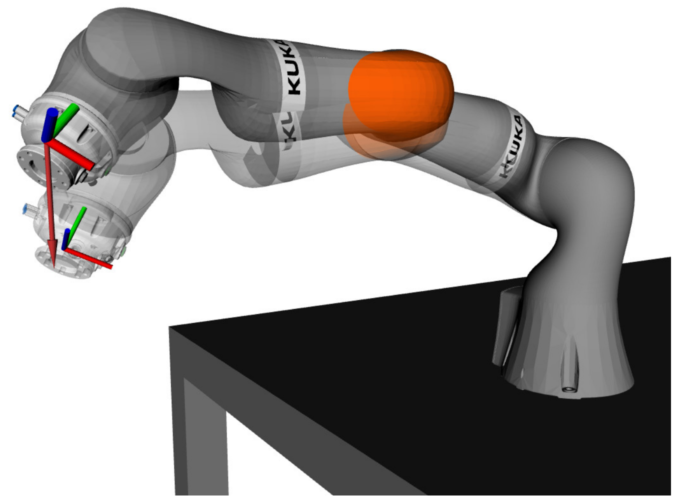

Fig. 4.1: Robot deflection prediction visualisation (exaggerated)

4.2 Reachability Study

The *reach* tool is principally a reachability analysis tool, however it can also optimise a given evaluation function for a set of poses. It can thus be used to perform studies to choose suitable regions of a robot's workspace according to stiffness metrics defined with **reflex**. This result can then be visualised interactively as shown in Figure 4.2. The desired input poses are represented by arrows, whose colour indicates what the maximum achievable value of the evaluation function is for that pose. Black arrows indicate unreachable poses. The user can choose a pose and the interface immediately shows the optimised inverse kinematics (IK) solution.

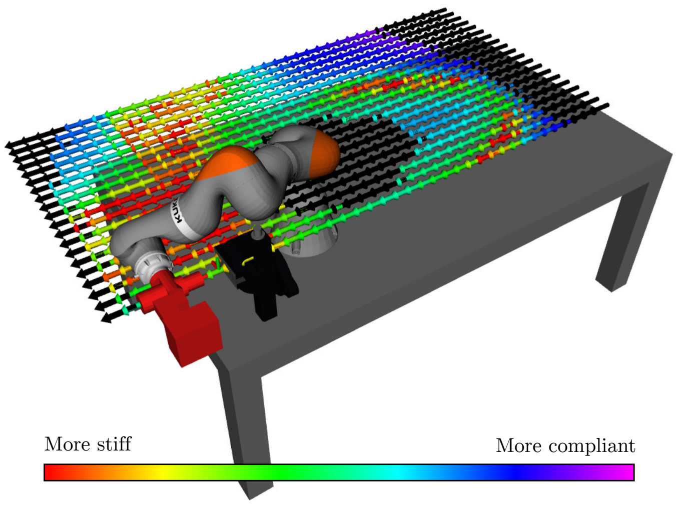

Fig. 4.2: Reach visualisation example using tolerance metric

Using additional tooling, different metrics can be compared, different target poses selected and evaluation function minima can be shown.

The validity of the results from these analysis tools is explored in Section 6. Before the analysis can be performed, the parameters of the model must be known.

5 Experiment: Joint Stiffness Identification

In order to use the robot stiffness model, some robot-specific parameters must first be identified. A Kuka LBR iiwa 14 R820 was used for all experiments. The kinematics are available from the manufacturer. The joint compliances (C_q) are not given, thus they must be determined experimentally.

5.1 Procedure

To determine the joint stiffness behaviour, both the torque at the joint and the joint displacement must be known. Fortunately, the robot has joint torque sensors, allowing for the simultaneous measurement of both values. It should be noted that link and passive joint compliance is not measured by these sensors. By applying various loads to the end-effector, the stiffness behaviour can be studied. The exact magnitude and direction of the applied wrench need not be known, since the joint torques are known. The robot was configured to use joint position control for all experiments.

Loads were applied by hand, by pushing on the robot's end-effector. Maximum joint torques were in excess of 20 % of the limits for each joint, such as to obtain sufficient displacement. The lack of accuracy and repeatability in applying the loads manually is of no concern, as both the independent and dependent variables are measured. The length of the loading phase was kept relatively short (below approximately 2 seconds), to avoid excessive integral wind-up. Any individual loading cycle was only applied from one direction and then released. This was achieved by pushing on the robot with the palm,

d. Available at https://github.com/thettasch/reflex_thesis so that on release no 'pulling' forces are generated. Care was taken to allow the robot to return to rest before applying the next loading cycle. Finally, loads were applied in as many directions as possible, to produce deflection at each joint. The added variance from manual loading is beneficial in ensuring robustness of the results.

Note that the external torque is computed internally by the robot controller, and does not include the joint controller output torque, as the name suggests. Gravity is compensated for by using the initial sensor readings as the zero point. The change in torques due to gravity under deflection is assumed to be minimal.

5.2 Joint Controller Behaviour

Figure 5.1 shows how the joint controller responds to an external disturbance. As the load is applied, the joint deflects and as the load is released, it returns towards zero, but overshoots due to integral wind-up. Eventually, the joint position error returns to zero.

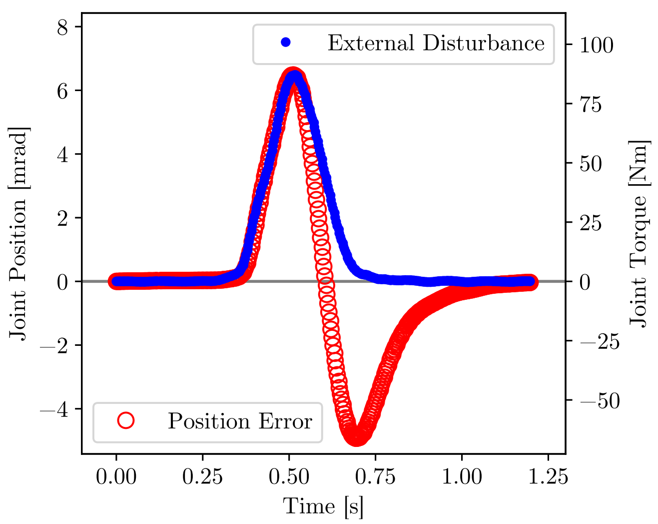

Fig. 5.1: Joint 1 disturbance reaction

Figure 5.2 shows the relationship between the joint position error and the externally applied torque (as measured by the robot), for repeated loading and unloading cycles, in both directions, for one joint. Figure 5.3 aims to clarify the observed behaviour. During loading, the joint position error proportionally increases with applied force. When the load is removed, the error returns towards zero, but overshoots due to the integral wind-up during the loading phase. Once the load is completely removed, the joint error eventually gets driven back to zero.

The maximum deflection is approximately linearly related to the applied joint torque. The slope of this curve will be referred to as the joint's loading compliance, as it represents the behaviour as a load is applied. It can be used to model the maximum expected deflection under loading. There are two main factors contributing to deviations from the ideal linear behaviour.

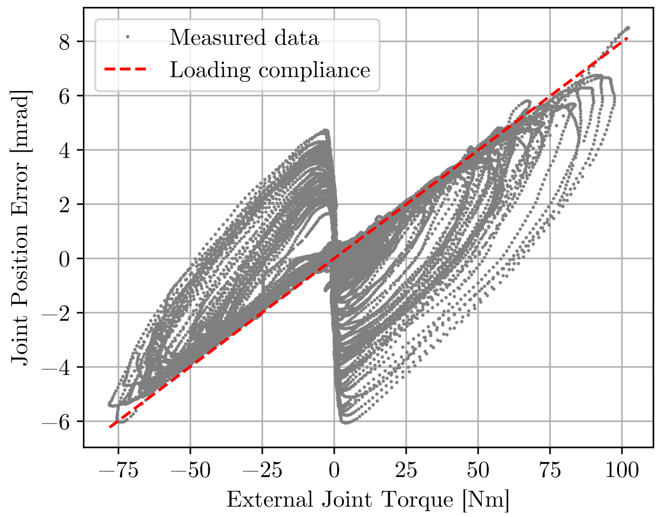

Fig. 5.2: External joint torque against joint position error, with a linear approximation for the compliance under loading (Joint 1)

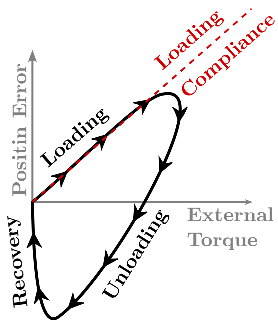

Fig. 5.3: Joint loading/unloading schematic

5.3 Deviation from Ideal Behaviour

Under pure proportional control (and zero mass), the load/unload curve would be purely linear, however the addition of an integral component introduces the hysteresis shown in Figure 5.3. The inertia of the links also affects the behaviour.

Under rapid loading, the inertia of the links reduces the maximum deflection. This effectively reduces the effective compliance.

Under very slow loading or extended application of load, the integral controller component drives the error lower. Note that once again, the effective compliance is reduced.

In both cases, the effective compliance is less than the loading compliance. Thus, the loading compliance can be used to determine the maximum deflection.

Note that the instantaneous relationship between torque and position error may exhibit higher or negative "compliance", especially during the recovery phase, due to lingering effects of previously applied loads. This effect is not explicitly taken into account.

5.4 Computed Stiffness Parameters

Applying the above procedure to every joint, their maximum compliances were determined. The loading compliance line was chosen such that 90 percent of points during the loading phase fall below it. This ensures robustness against outliers. The values are shown in Table 5.1 (additional plots in Appendix D). The maximum allowable joint torque is also shown, to illustrate how stronger joints are generally stiffer. The joint compliance matrix C_q from Equation 2.4 can be constructed as a diagonal matrix containing these values. Note that the joints are numbered conventionally, i.e. from the base towards the end-effector.

TABLE 5.1: Kuka LBR iiwa 14 R820 measured joint stiffnesses and maximum joint torques

Joint	**Maximum Torque** [N m]	**Minimum Stiffness** [kN m rad^{-1}]	**Maximum Compliance** [µrad N^{-1} m^{-1}]
1	320	13	80.
2	320	13	78
3	176	10.	100
4	176	6.2	160
5	120	5.4	190
6	40	3.5	280
7	40	4.2	240

5.5 Small Angle Assumption Validity

The VJM model relies on the small angle assumption $\sin(\theta) \approx \theta$. The following aims to show that this assumption is sufficiently accurate given the expected deflections for the robot in question.

The maximum expected joint deflection (under loading) may be computed as:

$$\delta q_{max} = c_q \tau_{max} \tag{5.1}$$

Then, the maximum relative error of the small angle approximation can be calculated as follows:

$$\text{rel err} = \frac{\sin(\delta q_{max}) - \delta q_{max}}{\sin(\delta q_{max})} \tag{5.2}$$

Performing these calculations for all joints yields the results shown in Table 5.2.

At most 0.13 ‱ of error is expected, in other words the results should be shown to at most 3 significant figures.

Now that the parameters to the stiffness model are all established, the stiffness optimisation can be applied. The following section validates whether this yields meaningful results.

TABLE 5.2: Maximum expected small angle approximation error for each joint

Joint	**Maximum Expected Deflection** [mrad]	**Small Angle Approximation Error** parts per thousand [‱]
1	25	0.11
2	25	0.10
3	18	0.051
4	28	0.13
5	20	0.070
6	11	0.021
7	9.6	0.015

6 Experiment: Stiffness Metric Verification

The relationship between the stiffness metric and the actual process performance must be established. If the metric is found to reliably predict the process accuracy, the process performance may be optimised through use of the stiffness metric. More explicitly, if the relationship between a measure of the process performance and the stiffness metric is monotonically increasing, then improvements in the stiffness metric (which can be analytically computed) directly translate into improvements of the process performance measure.

This relationship is established for one example application, namely through-hole drilling.

6.1 Experiment Setup

Drilling was chosen as a sample process, since it is straightforward to implement and a simple measure of performance exists: measuring the hole diameter. Moreover, since the primary process force is axial and the tolerance is radial, directional stiffness is not expected to sufficiently capture process performance. The exact methodology is provided below.

A custom robot cell was set up for this experiment. A conventional hand-drill was used as the end-effector on a Kuka LBR iiwa 14 R820 robot (see Figure 6.1). Note that the maximum achievable accuracy of this setup will be fundamentally limited due to compliance in the mounting and play in the drill. This is not deemed an issue, as the focus lies on the relative performance, not the absolute.

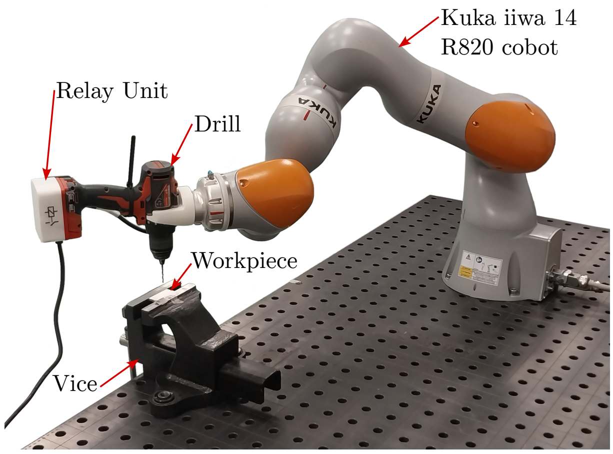

Fig. 6.1: Drilling robot cell

Holes were drilled in 50 × 20 × 5 mm aluminium blanks[e]. Figure 6.2 shows the workpiece[f] after drilling; notches are used to keep track of individual samples. The material is soft enough not to exceed the allowable load on the robot, while still producing enough reaction force to cause measurable deflection.

Fig. 6.2: Hole sample

6.2 Control Variables

In order to isolate the effect of the joint configuration on the process performance, as many extraneous variables as possible must be fixed. These pertain both to the drilling process, as well as to the robot motion planning and execution.

6.2.1 Drilling

Drilling is performed in 5 mm thick aluminium. The hole diameter is arbitrarily fixed at 3 mm. A high-speed steel (HSS) twist drill bit is employed. It is not exchanged throughout testing, to avoid the influence of variance between drill bits. Wear is not expected to pose an issue, as relatively few holes are drilled and aluminium is a relatively soft material (this claim is validated by the results in Table 6.1). The drill's speed is set to its maximum of 1800 rev min^{-1} (no-load). The feed speed is set to 2 mm s^{-1}, leading to an acceptable material removal rate [37]. Finally, the drill battery is changed every time the indicator reaches half full, to avoid a reduction in speed and power of the drill.

6.2.2 Motion planning

For motion planning, the *pilz_industrial_motion_planner* in the *MoveIt!* [38] framework was used. The drilling motions are purely linear. The end-effector Cartesian speed is capped at the feed rate. The exact motion planning pipeline is the same for all scenarios. Different configurations are achieved by seeding the motion plan differently, i.e. using different starting configurations.

6.3 Independent Variables

The primary independent variable which affects the stiffness behaviour is the joint configuration. Different joint configurations are achieved through two means; by moving the vice and workpiece to different locations/orientations and by choosing different IK solutions.

The robot has seven joints, and rotation around the drill axis can be regarded as an additional virtual joint, thus there are two additional degrees of freedom that may be leveraged to obtain different IK solutions. The vice holding the workpiece can easily be repositioned, by using the grid of holes in the table and quick locking bolts. The vice could be mounted either horizontally or vertically on the table (see Figure 6.3), allowing for a wide range of potential workpiece positions and orientations.

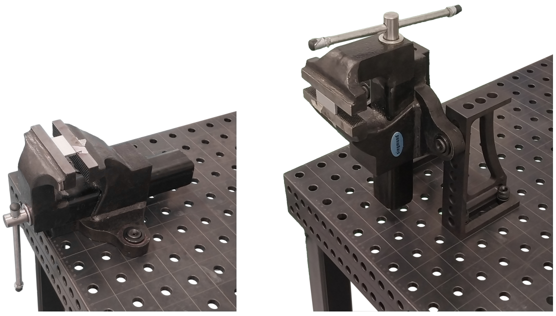

(a) Horizontal (b) Vertical

Fig. 6.3: Vice mounting orientations

6.4 Tolerance Metric Parameters

Before stiffness metric values can be computed, values must be chosen for the metric parameters. These are the positional tolerance and the expected load. Both are modelled at the tip of the drill bit, for convenience.

The position of the drill bit tip should fall within a cylindrical tolerance of the nominal centre axis of the hole. The magnitude of the allowable deviation is somewhat arbitrarily set to 0.5 mm. Since a linear stiffness model will be used, the magnitude is not important (see Section 3.3.2). The length of the cylinder is set to 5 mm, as this is the thickness of the material used. The full tolerance matrix is then obtained using Equation C.17.

The expected process force is chosen to be 50 ± 5 N in the axial direction. Once again, the magnitude is irrelevant, as only relative claims are made. For simplicity, the moment generated around the drilling axis is ignored.

Using these parameters a rough drilling tolerance metric is established. This is then used for joint configuration selection, and later validated against experimental results. From here on out, any mention of $m =$ ... will refer to this exact metric.

6.5 Joint Configuration Selection

A set of joint configurations was selected systematically. Poses with a wide range of stiffness metric values were chosen, with the aim of achieving as wide a spread of actual process performance as possible. The **reflex** framework discussed in Section 4 was used to find different poses near the maxima and minima of the stiffness metric and randomised IK poses were used to fill out the middle ground. Some candidate poses had to be eliminated, since motion planning failed for some (or all) of the five holes, due to collisions, singularities or joint limits being violated (see Section 7).

Two sample joint configurations are shown in Figure 6.4. All configurations are shown in Figure E.2 in Appendix E. These joint configurations form the initial conditions from which the motion planner then produces its trajectories.

e. Technical term for the material before machining.
f. Technical term for the part during/after machining.

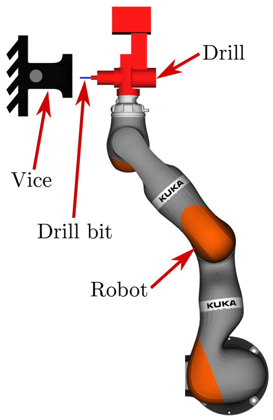

(a) More compliant pose
$m = 11$

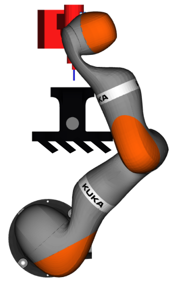

(b) More stiff pose
$m = 0.036$

Fig. 6.4: Top view of two sample joint configurations

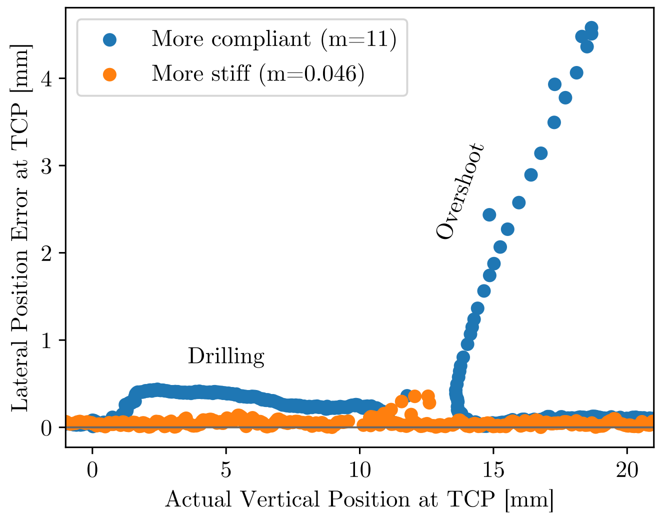

Fig. 6.5: Joint trajectory controller error during two drill cycles, showing increased error for higher compliance

A total of 14 joint configurations were chosen and one drilling sample (see Figure 6.2) produced for each. Eight workpiece positions, each with one to three IK solutions were used. For each sample, five holes were drilled, in order to control for random variations.

6.6 Measuring Performance

Depending on the tolerance requirements of the part, the performance may be measured differently.

For the purposes of this experiment, performance will be measured in two manners, one focusing on the robot controller performance and one on the actual hole.

6.6.1 Joint Trajectory Controller Performance

Firstly, the joint trajectory controller's error is logged, to obtain an understanding of how the force-induced displacement evolves during the process. By performing forward kinematics on both the desired and the actual joint states, the Cartesian error at the end-effector can be estimated. Only the lateral offset and the perpendicularity of the drill bit are of interest. Any errors in axial position and rotation around the drill axis do not affect the process. A sample plot of the lateral controller error is shown in Figure 6.5 for two different configurations. Note the error during drilling, followed by the large spike in error when the drill punches through the bottom of the material. In one case the error is significantly larger than the other, as predicted by the stiffness metric (a lower stiffness metric value indicates better performance).

The maximum error can be used as an indication of the performance, however the short duration of the spike with respect to the sampling frequency may cause deviation from the true maximum. For this reason, the 90^{th} percentile of the error was used as a more robust indication of the error experienced during the process. This measure intentionally does not account for kinematics errors and passive compliances, since these are not modelled and can therefore not be optimised for in any case. To ensure that the optimisation result is valid despite these unmodelled effects, a performance measure external to the robot is required.

6.6.2 Hole Diameter

The hole diameter is measured to obtain a better understanding of the actual precision of the process. Larger hole diameters indicate more undesirable wandering of the drill bit during the process. Ideally, the holes should be as small as possible (equal to the drill bit diameter). Absolute positioning is once again ignored, as it is strongly affected by kinematics errors.

The hole diameter was measured using a Mitutoyo MF-UF Measuring Microscope with an M Plan Apo 7.5X objective (Figure 6.6). The presence of burrs and frequent perpendicularity errors introduced some difficulty in the measurement process. Figure 6.7 shows macrographs of two holes. These images are for illustration only, as the focal plane is set too high to accurately perform measurements.

Fig. 6.6: Mitutoyo Measuring Microscope

Precautions were taken to obtain meaningful measurements. The diameter of each hole was measured twice, using different sets of points, to account for non-circularities to some degree. Three point measurements were used, since the position of the centre of the hole is unknown. The points could unfortunately not be in the same positions for each hole, due to burrs, occlusions and other artifacts. Measurements were

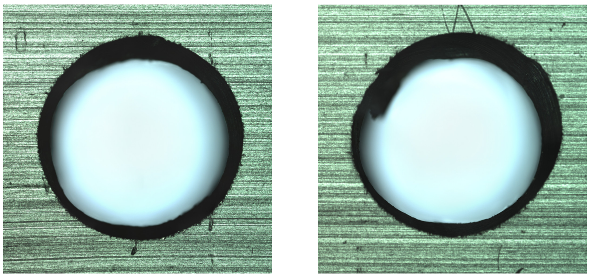

(a) Hole without burrs (b) Hole with internal burr

Fig. 6.7: Sample hole macrographs

taken between 0.2 mm and 0.6 mm below the upper surface (where the upper surface is the same as it was during drilling), to avoid the chamfers introduced during manual deburring. Perpendicularity of the holes was not measured; due to the relatively low thickness of the material, obtaining accurate measurements of the perpendicularity is infeasible.

6.7 Results

The results of the drilling tests for 70 holes are shown below. Only two outliers had to be partially removed; these were both confirmed to be results of user-error during the experiments.

Figure 6.8 shows the correlation between the lateral controller error and the stiffness metric. Note that lower values of the stiffness metric correlate with better performance, i.e. less controller tracking error. Points are grouped based on the workpiece position (WPP).

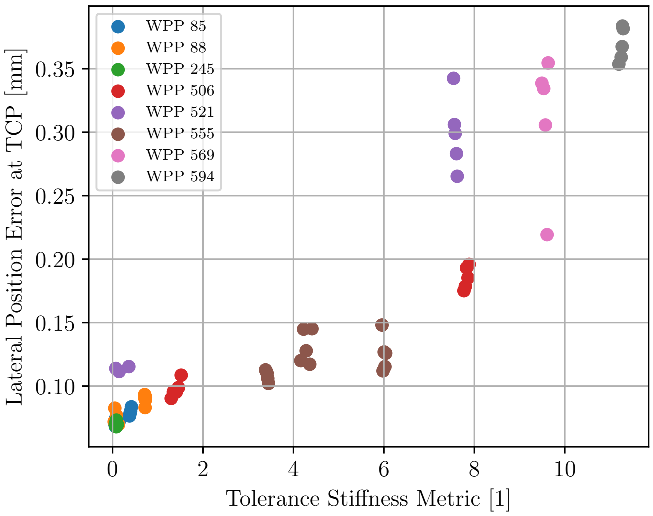

Fig. 6.8: Tolerance stiffness metric vs joint trajectory controller error, showing a strong positive correlation between the two (grouped by workpiece position)

The Spearman's rank correlation coefficient between the stiffness metric and the lateral controller error was found to be 0.93, indicating a strong positive correlation between the two values. Values close to one indicate that the data is monotonically increasing. This confirms that the stiffness metric can be used to predict the controller tracking performance, at least to some degree. The lateral error ranges from 380 µm to 68 µm. This indicates that there is indeed significant potential to reduce tracking error purely by changing the initial joint configuration.

Figure 6.9 shows the relationship between the stiffness metric and the measured hole diameters. There is significant variance of measured hole diameter for each sample, however the correlation is nevertheless apparent. Note that larger diameters indicate more deviation from the nominal hole size of 3 mm, i.e. worse performance.

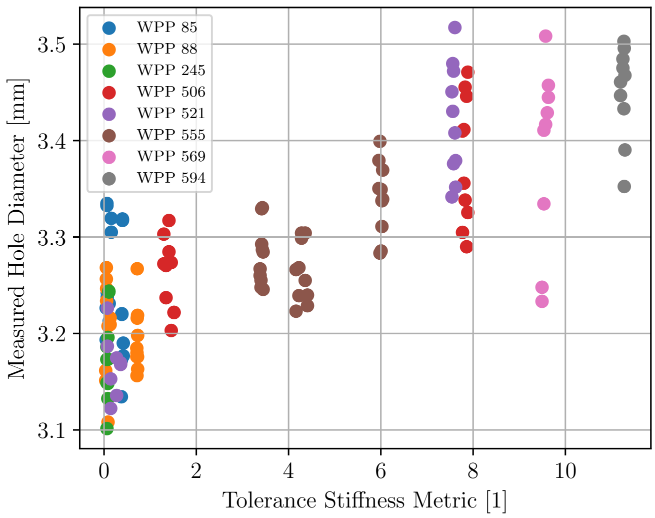

Fig. 6.9: Tolerance stiffness metric vs hole diameter, showing a positive correlation between the two (grouped by workpiece position)

Table 6.1 shows how well different stiffness metrics correlate with the drilling performance. Plots for each evaluated metric are shown in Appendix F. The following metrics are computed: the proposed tolerance metric, the screw stiffness in the axial direction and finally the isometry of the translational component of the stiffness matrix. The correlation with the distance between the workpiece and the robot base is also shown. The correlation with the sequence number, encoding the order the holes were drilled in, is also shown; the values are low enough to conclude that wear of the drill-bit had no significant impact on the data.

TABLE 6.1: Spearman's rank correlation coefficient between performance measures and various stiffness metrics

Metric	Correlation with Tracking Performance	Correlation with Hole Diameter
Toleranced	0.93	0.81
Axial Stiffness	0.60	0.59
Stiffness Isometry	0.84	0.70
Distance to Workpiece	0.76	0.59
Sequence Number	0.43	0.34

Note that the correlation is generally lower for the hole diameter, as there are more factors introducing noise to this measurement. The proposed tolerance stiffness metric exhibits the highest correlation with both measures of performance, in other words, it is most suitable for performance optimisation.

7 Discussion

There are many subtleties to consider before applying the above procedure to different processes.

7.1 Generalisability

The proposed stiffness metric is grounded in mathematical rigour, and is not data-driven, thus it is expected to generalise well to other processes, where the expected contact force (wrench) and the allowable tolerances are known. The tolerances should be trivial to identify based on engineering drawings of the final part. The expected wrench is more difficult to characterise, however most machining processes have been studied in detail, so obtaining an estimate should usually be possible. In cases where the magnitude of the expected load is unknown, the direction of the wrench can be used to compute a relative metric, which may still be used for optimisation (given that a linear stiffness model is used).

Beside the parameters of the stiffness metric, the robot model is required to be meaningful in order for the final values to have merit. Since these experiments were performed in joint position control mode, the model should also be applicable to a broad range of industrial robots, not just specialised cobots with joint torque sensors. Note that the joint compliance parameters are more easily measured for cobots, where for industrial robots a different methodology from the one shown here would be necessary.

The tolerance metric also suffers from two other flaws, which may hinder generalisability. Firstly, the tolerances are symmetric around the nominal position, however occasionally, asymmetric dimensional tolerances may be required by engineering drawings of the final part. For example, in some cases a deviation δx of a dimension x may be required to be bounded as follows: $0 < \delta x < \epsilon$. While this may be modelled using the tolerance metric by shifting the nominal value of x to $x + \frac{\epsilon}{2}$ (with a tolerance of $\pm\frac{\epsilon}{2}$), this is not strictly equivalent to the intended tolerance. Secondly, under addition of multiple tolerances, the combined tolerance grows more and more conservative. In other words, certain deflections may be considered to be out of tolerance, despite their adherence to all component tolerances (see the white region of Figure 3.2). This is a direct consequence of the use of the quadratic form in expressing tolerances. In theory, higher order polynomials may be used to more closely approximate the union between component tolerances, however this cannot be expressed neatly in matrix form (higher-order tensors would be required) and would lead to a drastic increase in number of parameters and computational cost.

7.2 Non-linearities

The actual robot stiffness behaviour is likely not purely linear. Large deflections, leading to significant displacement of rotational joints will lead to deviations from the small angle approximation (Section 5.5 shows this is not significant for the robot used here). Additionally, material behaviours in the robot structure may exhibit some non-linearities. Friction and stiction effects in the joints also lead to inaccuracies of the linear model. However, the final, largest contributor to non-linearity are the joint position controllers. These controllers are inherently non-linear, due to factors such as integral/derivative control and output/rate limits. There is a trade-off to be made. More complex models may more accurately predict robot behaviour, but require more extensive robot parameter identification.

The proposed stiffness metric remains useable no matter the complexity of the underlying robot stiffness model, since it acts on the predicted displacement. The linear model is useful for propagating uncertainty in the applied wrench, however this is by no means a necessity.

7.3 Controller Overshoot

The largest controller errors during drilling were experienced when punching through the bottom of the workpiece (Figure 6.5), due the sudden loss of normal force coupled with a wound-up integral control component. The size of these overshoot transients cannot be predicted with the modelling tools presented here, as it is a function of time, amongst other factors. Accounting for the exact overshoot behaviour would significantly increase overall complexity of the model. The stiffness metric is still expected to be useful for two reasons. Firstly, the direction of the overshoot should align roughly with the model prediction, thus if possible, the overshoot may be directed so as to not influence the process. For through-drilling, this means that the overshoot component should be aligned to the drill axis, with minimal effect on hole tolerance. Secondly, the vast majority of material removal occurs during the main contact phase and the short duration of the overshoot may cause disproportionately little material removal, leading to little actual impact on process performance.

7.4 Absolute Positioning Error

This report has been focused on the deflection of the end-effector due to external load and disregarded errors due to kinematics. However, kinematics errors during drilling were found to be significant, up to 10 mm with no loads applied. This was the case despite kinematics calibration prior to drilling. The kinematic error was not studied in detail, however it was likely in part due to sagging of the robot under gravity.

In real-world applications the absolute position accuracy of the tool is incredibly important, thus it is critical to also take kinematics into account when designing actual robotic machining setups. In certain cases, closed-loop control using external positioning sensors may even be necessary. Stiffness optimisation nevertheless remains relevant, as it may be used to decrease the effort required from the controllers.

For example, one might follow the following procedure:

1) Identify robot stiffness parameters, expected loads during the process and required tolerances

2) Use reachability/stiffness analysis to determine a suitable position and orientation of the workpiece, as well as a suitable joint-configuration

3) Perform in-depth kinematics calibration in the region around the chosen workpiece position/joint-configuration

4) Plan motions using calibrated kinematics

5) Execute motions (potentially using closed loop control for improved positioning accuracy)

By integrating stiffness optimisation in the planning phase, accuracy can still be improved and reliance on external sensors and closed-loop controllers minimised.

7.5 Closing the Contact Loop

So far the model has been used to predict deflection under some external force which is displacement invariant. For real processes, the force will likely vary with displacement. For example, once the drill bit enters a material, it too will resist lateral displacement, in other words, it becomes self-centring. In the case of drilling, the additional forces act to reduce displacement, however this may not be the case for other processes (e.g. climb-milling). Accounting for these additional forces may then become necessary. Under partial constraints, where the displacement is known in some directions, the reaction forces due to the robot stiffness can be computed (see Appendix A.6). Further research is required to establish the validity of these predictions and their applicability to predicting actual contact behaviour.

7.6 Restricted Workspace

Suitable stiffness optima (or near-optima) are only found in some parts of the robot's working envelope. Generally, serial robots will be stiffest when working close to their base. This naturally leads to a reduced useable workspace. The primary appeal of robotic machining with serial manipulators lies in their increased flexibility and large workspace. This conflict is physically unavoidable, vastly limiting the potential applications of robotic machining. Nevertheless, it is still useful to understand the stiffness behaviour of these robots, in order to make informed decisions regarding their applicability to solving a given problem.

7.7 Difficulty of Motion Planning

Optimising a robot's joint configuration for any metric may result in solutions that are near the boundary conditions of the optimisation. These are the joint limits, kinematic singularities and collisions. During testing, it was found that optimised stiffnesses tend to lie at these boundaries, leading to difficulties in motion planning in the vicinity of these points. This is partly an inherent problem of constrained optimisation, and partly an effect of the VJM stiffness model predicting infinite stiffness in certain directions when at singularity.

The current procedure of generating optimal starting poses often returns solutions where motion planning fails, due to proximity to the boundary conditions. To achieve consistently successful planning, the motion planner itself would have to be aware of the stiffness metric, so that the whole trajectory and not just the initial pose may be optimised and adjusted.

7.8 Potential Future Work

Finally, some regions of potentially interesting future research are summarised below.

Robot stiffness models may be improved and studied further:

- Experimental comparison between the joint and link deflections, to establish the accuracy of the VJM model.
- Verifying that the expression for partially-constrained stiffness behaviour developed in Appendix A.6 is valid.
- Addition of link and tool compliances to the VJM model through use of virtual, multi-degree-of-freedom joints.
- More elaborate modelling of the joint stiffness behaviours, including time-dependent effects due to integral control.

The tolerance stiffness metric may be studied and the stiffness optimisation procedure developed further:

- Experimentally confirming that the tolerance stiffness metric is applicable to different processes (e.g. milling or grinding).
- Verification that the absolute tolerance metric can predict whether or not a process will comply to its tolerances.
- Integration of the metric into an optimising motion planner, for more reliable planning.
- Development of a joint-compliance measuring procedure for industrial robots.
- Studying the relationship between tool deflection and the resultant material removal and thus dimensional error of the workpiece.
- Establishing whether more accurate estimates of the process force lead to better correlation between the metric and the performance.
- Use of the metric during motion execution (i.e. within the controllers), to alter joint-configuration or even joint-stiffness, potentially incorporating joint-torque sensor readings to estimate the wrench at the end-effector.

8 Conclusion

A new means of evaluating the suitability of robot joint configurations for contact processes is proposed. First, the robot joint stiffness behaviour is identified in order to predict the displacements experienced under contact. Then, it was shown that the proposed stiffness metric is strongly correlated with the process performance for the specific case of through-hole drilling. The process performance can thus be improved by numerically optimising the stiffness metric over any additional degrees of freedom of the overall system. These can stem from an over actuated robot system, under-constrained end-effector pose, and choices in end-effector, workpiece or robot mounting positions. While the validation was performed only on drilling, it is expected that the stiffness metric is applicable to any well-understood contact process.

The stiffness metric may be useful in two situations. During design of a robot cell, it may aid in selection of robot and/or workpiece placement, as well as design of the end-effector for best stiffness performance. Secondly, the metric may be used as a cost function during motion planning. In both cases, no modification to existing robot hardware or control software is required and thus improvements in process accuracy are effectively free of cost. Some constraints and limitations exist, possibly limiting the maximum achievable improvement in stiffness. Furthermore, a flexible software framework for enabling these analyses and optimisations was created.

During experimentation, the joint trajectory tracking error was found to vary by a factor of more than 5 between different joint configurations (see Figure 6.8). Additionally, the proposed tolerance stiffness metric was found to have the best correlation with both joint trajectory controller error and hole diameter, when compared to existing methods. Combined, these results confirm not only that the proposed stiffness metric is meaningful for optimisation, but also that stiffness optimisation can potentially significantly improve positioning accuracy under load.

References

[1] W. Ji and L. Wang, "Industrial robotic machining: a review," *The International Journal of Advanced Manufacturing Technology*, vol. 103, no. 1-4, pp. 1239–1255, Jul. 2019. [Online]. Available: http://link.springer.com/10.1007/s00170-019-03403-z

[2] U. Schneider, M. Drust, M. Ansaloni, C. Lehmann, M. Pellicciari, F. Leali, J. W. Gunnink, and A. Verl, "Improving robotic machining accuracy through experimental error investigation and modular compensation," *The International Journal of Advanced Manufacturing Technology*, vol. 85, no. 1-4, pp. 3–15, Jul. 2016. [Online]. Available: http://link.springer.com/10.1007/s00170-014-6021-2

[3] N. Shen, Z. Guo, J. Li, L. Tong, and K. Zhu, "A practical method of improving hole position accuracy in the robotic drilling process," *The International Journal of Advanced Manufacturing Technology*, vol. 96, no. 5-8, pp. 2973–2987, May 2018. [Online]. Available: http://link.springer.com/10.1007/s00170-018-1776-5

[4] S. Caro, S. Garnier, B. Furet, A. Klimchik, and A. Pashkevich, "Workpiece placement optimization for machining operations with industrial robots," in *2014 IEEE/ASME International Conference on Advanced Intelligent Mechatronics*. Besacon: IEEE, Jul. 2014, pp. 1716–1721. [Online]. Available: https://ieeexplore.ieee.org/document/6878331

[5] Y. Guo, H. Dong, and Y. Ke, "Stiffness-oriented posture optimization in robotic machining applications," *Robotics and Computer-Integrated Manufacturing*, vol. 35, pp. 69–76, Oct. 2015. [Online]. Available: https://linkinghub.elsevier.com/retrieve/pii/S0736584515000241

[6] G.-C. Vosniakos and E. Matsas, "Improving feasibility of robotic milling through robot placement optimisation," *Robotics and Computer-Integrated Manufacturing*, vol. 26, no. 5, pp. 517–525, Oct. 2010. [Online]. Available: https://linkinghub.elsevier.com/retrieve/pii/S0736584510000256

[7] J. Jiao, W. Tian, L. Zhang, B. Li, J. Hu, Y. Li, D. Li, and J. Zhang, "Variable Stiffness Identification and Configuration Optimization of Industrial Robots for Machining Tasks," *Chinese Journal of Mechanical Engineering*, vol. 35, no. 1, p. 115, Dec. 2022. [Online]. Available: https://cjme.springeropen.com/articles/10.1186/s10033-022-00778-1

[8] C. Dumas, S. Caro, M. Cherif, S. Garnier, and B. Furet, "Joint stiffness identification of industrial serial robots," *Robotica*, vol. 30, no. 4, pp. 649–659, Jul. 2012. [Online]. Available: https://www.cambridge.org/core/product/identifier/S0263574711000932/type/journal_article

[9] Z. Zhang, J. Xiao, H. Liu, and T. Huang, "Base placement optimization of a mobile hybrid machining robot by stiffness analysis considering reachability and nonsingularity constraints," *Chinese Journal of Aeronautics*, vol. 36, no. 11, pp. 398–416, Nov. 2023. [Online]. Available: https://linkinghub.elsevier.com/retrieve/pii/S1000936122003077

[10] H. Jamshidifar, A. Khajepour, B. Fidan, and M. Rushton, "Kinematically-Constrained Redundant Cable-Driven Parallel Robots: Modeling, Redundancy Analysis, and Stiffness Optimization," *IEEE/ASME Transactions on Mechatronics*, vol. 22, no. 2, pp. 921–930, Apr. 2017. [Online]. Available: http://ieeexplore.ieee.org/document/7782297/

[11] C. Ye, J. Yang, H. Zhao, and H. Ding, "Task-dependent workpiece placement optimization for minimizing contour errors induced by the low posture-dependent stiffness of robotic milling," *International Journal of Mechanical Sciences*, vol. 205, p. 106601, Sep. 2021. [Online]. Available: https://linkinghub.elsevier.com/retrieve/pii/S0020740321003362

[12] Z. Liao, Q.-H. Wang, H. Xie, J.-R. Li, X. Zhou, and P. Hua, "Optimization of Robot Posture and Workpiece Setup in Robotic Milling With Stiffness Threshold," *IEEE/ASME Transactions on Mechatronics*, vol. 27, no. 1, pp. 582–593, Feb. 2022. [Online]. Available: https://ieeexplore.ieee.org/document/9385906/

[13] Y. Xue, Z. Sun, S. Liu, D. Gao, and Z. Xu, "Stiffness-Oriented Placement Optimization of Machining Robots for Large Component Flexible Manufacturing System," *Machines*, vol. 10, no. 5, p. 389, May 2022. [Online]. Available: https://www.mdpi.com/2075-1702/10/5/389

[14] Q. Fan, Z. Gong, B. Tao, Y. Gao, Z. Yin, and H. Ding, "Base position optimization of mobile manipulators for machining large complex components," *Robotics and Computer-Integrated Manufacturing*, vol. 70, p. 102138, Aug. 2021. [Online]. Available: https://linkinghub.elsevier.com/retrieve/pii/S0736584521000235

[15] H. Xie, W.-l. Li, D.-H. Zhu, Z.-p. Yin, and H. Ding, "A Systematic Model of Machining Error Reduction in Robotic Grinding," *IEEE/ASME Transactions on Mechatronics*, vol. 25, no. 6, pp. 2961–2972, Dec. 2020. [Online]. Available: https://ieeexplore.ieee.org/document/9109573/

[16] F. Tian, C. Lv, Z. Li, and G. Liu, "Modeling and control of robotic automatic polishing for curved surfaces," *CIRP Journal of Manufacturing Science and Technology*, vol. 14, pp. 55–64, Aug. 2016. [Online]. Available: https://linkinghub.elsevier.com/retrieve/pii/S1755581716300311

[17] V. Pandiyan, W. Caesarendra, T. Tjahjowidodo, and G. Praveen, "Predictive Modelling and Analysis of Process Parameters on Material Removal Characteristics in Abrasive Belt Grinding Process," *Applied Sciences*, vol. 7, no. 4, p. 363, Apr. 2017. [Online]. Available: http://www.mdpi.com/2076-3417/7/4/363

[18] B. Zhang, S. Wu, D. Wang, S. Yang, F. Jiang, and C. Li, "A review of surface quality control technology for robotic abrasive belt grinding of aero-engine blades," *Measurement*, vol. 220, p. 113381, Oct. 2023. [Online]. Available: https://linkinghub.elsevier.com/retrieve/pii/S0263224123009454

[19] Y. Bu, W. Liao, W. Tian, J. Zhang, and L. Zhang, "Stiffness analysis and optimization in robotic drilling application," *Precision Engineering*, vol. 49, pp. 388–400, Jul. 2017. [Online]. Available: https://linkinghub.elsevier.com/retrieve/pii/S0141635916304184

[20] J. Gotlih, M. Brezocnik, and T. Karner, "Stiffness-Based Cell Setup Optimization for Robotic Deburring with a Rotary Table," *Applied Sciences*, vol. 11, no. 17, p. 8213, Sep. 2021. [Online]. Available: https://www.mdpi.com/2076-3417/11/17/8213

[21] N. C. N. Doan and W. Lin, "Optimal robot placement with consideration of redundancy problem for wrist-partitioned 6R articulated robots," *Robotics and Computer-Integrated Manufacturing*, vol. 48, pp. 233–242, Dec. 2017. [Online]. Available: https://linkinghub.elsevier.com/retrieve/pii/S0736584516301363

[22] T. Cvitanic, V. Nguyen, and S. N. Melkote, "Pose optimization in robotic machining using static and dynamic stiffness models," *Robotics and Computer-Integrated Manufacturing*, vol. 66, p. 101992, Dec. 2020. [Online]. Available: https://linkinghub.elsevier.com/retrieve/pii/S0736584520302039

[23] C. Dumas, S. Caro, S. Garnier, and B. Furet, "Workpiece Placement Optimization of Six-Revolute Industrial Serial Robots for Machining Operations," in *Volume 2: Applied Fluid Mechanics; Electromechanical Systems and Mechatronics; Advanced Energy Systems; Thermal Engineering; Human Factors and Cognitive Engineering*. Nantes, France: American Society of Mechanical Engineers, Jul. 2012, pp. 419–428. [Online]. Available: https://asmedigitalcollection.asme.org/ESDA/proceedings/ESDA2012/44854/419/230739

[24] J. Salisbury, "Active stiffness control of a manipulator in cartesian coordinates," in *1980 19th IEEE Conference on Decision and Control including the Symposium on Adaptive Processes*. Albuquerque, NM, USA: IEEE, Dec. 1980, pp. 95–100. [Online]. Available: http://ieeexplore.ieee.org/document/4046624/

[25] G. Alici and B. Shirinzadeh, “Enhanced stiffness modeling, identification and characterization for robot manipulators,” *IEEE Transactions on Robotics*, vol. 21, no. 4, pp. 554–564, Aug. 2005. [Online]. Available: http://ieeexplore.ieee.org/document/1492472/

[26] A. Klimchik, S. Caro, B. Furet, and A. Pashkevich, “Complete Stiffness Model for a Serial Robot:,” in *Proceedings of the 11th International Conference on Informatics in Control, Automation and Robotics*. Vienna, Austria: SCITEPRESS - Science and and Technology Publications, 2014, pp. 192–202. [Online]. Available: http://www.scitepress.org/DigitalLibrary/Link.aspx?doi=10.5220/0005098701920202

[27] V. Portman, “Robot stiffness evaluability problem: Solution by Schur complements and collinear stiffness values,” *Mechanism and Machine Theory*, vol. 161, p. 104297, Jul. 2021. [Online]. Available: https://linkinghub.elsevier.com/retrieve/pii/S0094114X21000550

[28] S. Abdolshah, D. Zanotto, G. Rosati, and S. K. Agrawal, “Optimizing Stiffness and Dexterity of Planar Adaptive Cable-Driven Parallel Robots,” *Journal of Mechanisms and Robotics*, vol. 9, no. 3, p. 031004, Jun. 2017. [Online]. Available: https://asmedigitalcollection.asme.org/mechanismsrobotics/article/doi/10.1115/1.4035681/472662/Optimizing-Stiffness-and-Dexterity-of-Planar

[29] İ. Görgülü and M. İ. C. Dede, “A New Stiffness Performance Index: Volumetric Isotropy Index,” *Machines*, vol. 7, no. 2, p. 44, Jun. 2019. [Online]. Available: https://www.mdpi.com/2075-1702/7/2/44

[30] G. Carbone and M. Ceccarelli, “Comparison of indices for stiffness performance evaluation,” *Frontiers of Mechanical Engineering in China*, vol. 5, no. 3, pp. 270–278, Sep. 2010. [Online]. Available: http://link.springer.com/10.1007/s11465-010-0023-z

[31] Qingsong Xu and Yangmin Li, “GA-Based Architecture Optimization of a 3-PUU Parallel Manipulator for Stiffness Performance,” in *2006 6th World Congress on Intelligent Control and Automation*. Dalian, China: IEEE, 2006, pp. 9099–9103. [Online]. Available: http://ieeexplore.ieee.org/document/1713760/

[32] F. Petit and A. Albu-Schaffer, “Cartesian impedance control for a variable stiffness robot arm,” in *2011 IEEE/RSJ International Conference on Intelligent Robots and Systems*. San Francisco, CA: IEEE, Sep. 2011, pp. 4180–4186. [Online]. Available: http://ieeexplore.ieee.org/document/6094736/

[33] F. Stella, J. Hughes, D. Rus, and C. Della Santina, “Prescribing Cartesian Stiffness of Soft Robots by Co-Optimization of Shape and Segment-Level Stiffness,” *Soft Robotics*, vol. 10, no. 4, pp. 701–712, Aug. 2023. [Online]. Available: https://www.liebertpub.com/doi/10.1089/soro.2022.0025

[34] A. Albu-Schaffer, M. Fischer, G. Schreiber, F. Schoeppe, and G. Hirzinger, “Soft robotics: what Cartesian stiffness can obtain with passively compliant, uncoupled joints?” in *2004 IEEE/RSJ International Conference on Intelligent Robots and Systems (IROS) (IEEE Cat. No.04CH37566)*, vol. 4. Sendai, Japan: IEEE, 2004, pp. 3295–3301. [Online]. Available: http://ieeexplore.ieee.org/document/1389925/

[35] S. Chitta, “MoveIt!: An Introduction,” in *Robot Operating System (ROS): The Complete Reference (Volume 1)*, ser. Studies in Computational Intelligence, A. Koubaa, Ed. Cham: Springer International Publishing, 2016, pp. 3–27. [Online]. Available: https://doi.org/10.1007/978-3-319-26054-9_1

[36] “ros-industrial/reach_ros2,” Mar. 2025, original-date: 2023-05-09T18:23:49Z. [Online]. Available: https://github.com/ros-industrial/reach_ros2

[37] V. P. Astakhov, “Drilling,” in *Modern Machining Technology*. Elsevier, 2011, pp. 79–212. [Online]. Available: https://linkinghub.elsevier.com/retrieve/pii/B9780857090997500022

[38] D. T. Coleman, I. A. Sucan, S. Chitta, and N. Correll, “Reducing the Barrier to Entry of Complex Robotic Software: a MoveIt! Case Study,” 2014. [Online]. Available: https://aisberg.unibg.it//handle/10446/87657

[39] A. Das, “New methods to compute the generalized chi-square distribution,” Feb. 2025, arXiv:2404.05062 [stat]. [Online]. Available: http://arxiv.org/abs/2404.05062

[40] R. B. Davies, “Algorithm AS 155: The Distribution of a Linear Combination of 2 Random Variables,” *Applied Statistics*, vol. 29, no. 3, p. 323, 1980. [Online]. Available: https://www.jstor.org/stable/10.2307/2346911?origin=crossref

[41] R. C. Martin, J. Grenning, S. Brown, and K. Henney, *Clean Architecture: a craftsman’s guide to software structure and design*, ser. Robert C. Martin series. Boston Columbus Indianapolis New York San Francisco Amsterdam Cape Town Dubai London Madrid Milan Munich Paris Montreal Toronto Delhi Mexico City São Paulo Sydney Hong Kong Seoul Singapore Taipei Tokyo: Prentice Hall, 2018.

Appendix A
Linear Compliance

A.1 Representing Wrenches and Deflections

In order to model the Cartesian stiffness behaviour of compliant systems, there must be some structured way to represent wrenches (forces and moments) applied to a system, as well as the resulting deflection (both linear and angular). Screw theory provides us with a convenient way to represent these quantities, namely with a vector of length 6, containing first the linear components, then the angular ones. Thus a wrench can be written as:

$$F = \begin{bmatrix} \mathcal{F} & M \end{bmatrix}^T = \begin{bmatrix} \mathcal{F}_x & \mathcal{F}_y & \mathcal{F}_z & M_x & M_y & M_z \end{bmatrix}^T \tag{A.1}$$

And a small deflection can be written as:

$$\delta X = \begin{bmatrix} \delta \mathcal{X} & \delta \Theta \end{bmatrix}^T = \begin{bmatrix} \delta x & \delta y & \delta z & \delta\theta_x & \delta\theta_y & \delta\theta_z \end{bmatrix}^T \tag{A.2}$$

It should be noted that these vectors are not dimensionally consistent and that as a consequence, operations such as the norm cannot be directly applied to them.

A.2 The Cartesian Compliance Matrix

The compliance of a point can be represented as a 6×6 matrix C_x, to relate the wrench applied to the point with the resulting displacement:

$$\delta X = C_x F \tag{A.3}$$

This model is incredibly powerful. It can be used to express any linear stiffness behaviours. As an example, the model could be used to express the behaviour at a point on an idealised beam.

A.2.1 Combination

The compliance of two systems at one point can be combined.

To combine the compliance C_A of one system and C_B of another, independent system, one must realise that the following equations hold:

$$F_{combined} = F_A + F_B \tag{A.4}$$

$$\delta X_{combined} = \delta X_A = \delta X_B \tag{A.5}$$

We can thus write:

$$F_{combined} = C_A^{-1} \delta X_A + C_B^{-1} \delta X_B \tag{A.6}$$

$$F_{combined} = \left(C_A^{-1} + C_B^{-1}\right) \delta X_{combined} \tag{A.7}$$

Finally:

$$C_{combined}^{-1} = C_A^{-1} + C_B^{-1} \tag{A.8}$$

A.3 Transforming Wrenches

A.3.1 Offsetting the application point

If wrench F_A is applied at point A of some solid body, then there must be some equivalent wrench F_B, applied at point B (on the same solid body), which has the same effect.

Let the vector pointing from A to B be:

$$r_{BA} = \begin{bmatrix} r_x & r_y & r_z \end{bmatrix}^T \tag{A.9}$$

The forces $\mathcal{F}_A$ and $\mathcal{F}_B$ must be equal. The force at A generates a moment around B, which must be accounted for in the expression for F_B. Specifically:

$$\mathcal{F}_B = \mathcal{F}_A \tag{A.10}$$

$$M_B = M_A + \mathcal{F}_A \times r_{BA} = M_A - r_{BA} \times \mathcal{F}_A \tag{A.11}$$

Note that using the cross product matrix form of r

$$[r]_\times = \begin{bmatrix} 0 & -r_z & r_y \\ r_z & 0 & -r_x \\ -r_y & r_x & 0 \end{bmatrix} \tag{A.12}$$

cross products may be written as matrix multiplication:

$$r \times x = [r]_\times x \tag{A.13}$$

$$x \times r = -[r]_\times x \tag{A.14}$$

Now we can express offsetting of the wrench as a simple transformation:

$$_w\mathcal{H}_{BA} = \begin{bmatrix} I & 0 \\ -[r_{BA}]_\times & I \end{bmatrix} \tag{A.15}$$

$$F_B = {}_w\mathcal{H}_{BA} F_A \tag{A.16}$$

A.3.2 Transforming between coordinate frames

It may be useful to express a wrench in different coordinate frames. Let F^C be a wrench expressed in coordinate frame C and Let F^D be the same wrench expressed in coordinate frame D.

The Rotation from frame C to frame D can be expressed as R_{DC}, a 3x3 matrix. The offset between the two coordinate frames does not affect the wrench, assuming it is still applied at the same point.

The transformation can be expressed as:

$$\mathcal{H}^{DC} = \begin{bmatrix} R_{DC} & 0 \\ 0 & R_{DC} \end{bmatrix} \tag{A.17}$$

$$F^D = \mathcal{H}^{DC} F^C \tag{A.18}$$

A.3.3 Combined transformation

Combining the two transformations, we get:

$$
{}_w\mathcal{H}_{BA}^{DC} = \mathcal{H}^{DC}{}_w\mathcal{H}_{BA}^{C} \tag{A.19}
$$

$$
= \begin{bmatrix} R_{DC} & 0 \\ -R_{DC}[r_{BA}^{C}]_\times & R_{DC} \end{bmatrix} \tag{A.20}
$$

The inverse of this transformation can be represented as:

$$
{}_w\mathcal{H}_{AB}^{CD} = \left({}_w\mathcal{H}_{BA}^{DC}\right)^{-1} \tag{A.21}
$$

$$
= \begin{bmatrix} R_{DC}^T & 0 \\ [r_{BA}^{C}]_\times R_{DC}^T & R_{DC}^T \end{bmatrix} \tag{A.22}
$$

A.4 Transforming Twists

Twists transform similarly to wrenches:

$$
\delta\mathcal{X}_B = \delta\mathcal{X}_A + \delta\Theta_A \times r_{BA} = \delta\mathcal{X}_A - r_{BA} \times \delta\Theta_A \tag{A.23}
$$

$$
\delta\Theta_B = \delta\Theta_A \tag{A.24}
$$

Thus the transformation matrix for an offset is:

$$
\delta X_B = {}_x\mathcal{H}_{BA}\delta X_A \tag{A.25}
$$

$$
{}_x\mathcal{H}_{BA} = \begin{bmatrix} I & -[r_{BA}]_\times \\ 0 & I \end{bmatrix} \tag{A.26}
$$

The combined transform for a twist is:

$$
{}_x\mathcal{H}_{BA}^{DC} = \begin{bmatrix} R_{DC} & -R_{DC}[r_{BA}^{C}]_\times \\ 0 & R_{DC} \end{bmatrix} \tag{A.27}
$$

With the inverse being:

$$
{}_x\mathcal{H}_{AB}^{CD} = \begin{bmatrix} R_{DC}^T & [r_{BA}^{C}]_\times R_{DC}^T \\ 0 & R_{DC}^T \end{bmatrix} \tag{A.28}
$$

A.4.1 Relation to wrench transforms

It should be noted that wrench and twist transforms are related as follows:

$$
\left({}_x\mathcal{H}_{BA}^{DC}\right)^T = \left({}_w\mathcal{H}_{BA}^{DC}\right)^{-1} \tag{A.29}
$$

$$
\left({}_x\mathcal{H}_{BA}^{DC}\right)^T = {}_w\mathcal{H}_{AB}^{CD} \tag{A.30}
$$

A.5 Transforming Compliance Matrices

Compliance at point A in frame C is given as:

$$
\delta X_A^C = C_A^C F_A^C \tag{A.31}
$$

Thus the equivalent compliance at point B in frame D can be computed as:

$$
\delta X_A^C = {}_x\mathcal{H}_{AB}^{CD}\delta X_B^D = C_A^C{}_w\mathcal{H}_{AB}^{CD}F_B^D = C_A^C F_A^C \tag{A.32}
$$

$$
\delta X_B^D = \left({}_x\mathcal{H}_{AB}^{CD}\right)^{-1} C_A^C{}_w\mathcal{H}_{AB}^{CD}F_B^D \tag{A.33}
$$

$$
\delta X_B^D = {}_x\mathcal{H}_{BA}^{DC}C_A^C{}_w\mathcal{H}_{AB}^{CD}F_B^D \tag{A.34}
$$

$$
\delta X_B^D = C_B^D F_B^D \tag{A.35}
$$

$$
\tag{A.36}
$$

More simply:

$$
C_B^D = \left({}_x\mathcal{H}_{BA}^{DC}\right) C_A^C \left({}_w\mathcal{H}_{AB}^{CD}\right) \tag{A.37}
$$

$$
= \left({}_w\mathcal{H}_{AB}^{CD}\right)^T C_A^C \left({}_w\mathcal{H}_{AB}^{CD}\right) \tag{A.38}
$$

This transform may be used to obtain the compliance at an arbitrary point on the end-effector, in any given coordinate frame.

A.6 Partial Constraints

The compliance model accepts a wrench as an input, and outputs the displacement. In some cases, the end-effector may be rigidly constrained, thus some components of the displacement and wrench are known, and some not. By reorganising the rows of the wrench and displacement such that the known and unknown terms are grouped, one can obtain the following equation:

$$
\begin{bmatrix} \delta X_{\text{known}} \\ \delta X_{\text{unknown}} \end{bmatrix} = \begin{bmatrix} C_{ku} & C_{kk} \\ C_{uu} & C_{uk} \end{bmatrix} \begin{bmatrix} F_{\text{unknown}} \\ F_{\text{known}} \end{bmatrix} \tag{A.39}
$$

Now it should be noted that the known wrench components are necessarily equal to zero in the absence of friction. Under this assumption, the above equation can be simplified to:

$$
\begin{bmatrix} \delta X_{\text{known}} \\ \delta X_{\text{unknown}} \end{bmatrix} = \begin{bmatrix} C_{ku} \\ C_{uu} \end{bmatrix} F_{\text{unknown}} \tag{A.40}
$$

Since each unknown displacement is paired with a known wrench component (and vice-versa), C_{ku} must be square. Thus:

$$
F_{\text{unknown}} = C_{ku}^{-1}\delta X_{\text{known}} \tag{A.41}
$$

To simplify the row rearrangement, a matrix P can be employed, such that the following holds:

$$P\delta X = \delta X_{\text{known}} \tag{A.42}$$

$$F = P^T F_{\text{unknown}} \tag{A.43}$$

$$C_{ku} = P C_x P^T \tag{A.44}$$

Matrix P is simply an $n \times 6$ matrix, where n is the number of known wrench components (or unknown displacement components). It can be constructed by removing rows from an identity matrix.

So finally, the reaction wrench can be computed from the partially known displacement:

$$F = P^T \left(P C_x P^T \right)^{-1} P\delta X_{\text{partial}} \tag{A.45}$$

The full displacment can then simply be computed as usual:

$$\delta X_{\text{full}} = C_x F \tag{A.46}$$

A.6.1 Example

For example, if the tip of the robot is positionally constrained using a ball joint, the P matrix is as follows. The rotational components of the wrench are known to be zero, but the linear forces are not.

$$P = \begin{bmatrix} 0 & 0 & 0 & 1 & 0 & 0 \\ 0 & 0 & 0 & 0 & 1 & 0 \\ 0 & 0 & 0 & 0 & 0 & 1 \end{bmatrix} \tag{A.47}$$

The resulting extracted partial matrices are:

$$P\delta X = \delta X_{\text{linear}} = \delta \mathcal{X} \tag{A.48}$$

$$F = P^T F_{\text{linear}} = P^T \mathcal{F} \tag{A.49}$$

$$C_{\text{tran}} = P C_x P^T \tag{A.50}$$

Thus the linear reaction forces can be calculated from the applied displacement as follows:

$$\mathcal{F} = C_{\text{tran}}^{-1} P \delta \mathcal{X} \tag{A.51}$$

Appendix B
Robot Model

B.1 Derivation of the simplified VJM

The robot Jacobian is defined as:

$$\dot{X}_{tip}^{base} = J(q)\dot{q} \tag{B.1}$$

Where the Cartesian velocity (linear and angular) of the end-effector, is $\dot{X}$. The joint configuration is q and the speeds of the joints is $\dot{q}$.

Additionally, the jacobian can be used to equate the joint efforts (torques or forces) τ to Cartesian space, i.e. the wrench F:

$$\tau = J(q)^T F_{tip}^{base} \tag{B.2}$$

We assume that each joint is independent and behaves like a linear spring, with a compliance of $c_{q,n}$, thus:

$$\delta q_n = c_{q,n} \tau_n \tag{B.3}$$

$$\delta q = \text{diag}(c_q)\tau \tag{B.4}$$

Where $C_q = \text{diag}(c_q)$ is a diagonal matrix of the joint compliances.

Thus the joint displacement δq under load F is:

$$\delta q = C_q J(q + \delta q)^T F_{tip}^{base} \tag{B.5}$$

$$\delta q \approx C_q J(q)^T F_{tip}^{base} \tag{B.6}$$

The translational/rotational behaviour at the end-effector is:

$$\dot{X}_{tip}^{base} = J(q + \delta q)\dot{q} \tag{B.7}$$

For small changes in q, the following approximation can be made for the end-effector displacement:

$$\delta X_{tip}^{base} \approx J(q)\delta q \tag{B.8}$$

Thus:

$$\delta X_{tip}^{base} \approx J(q) C_q J(q)^T F_{tip}^{base} \tag{B.9}$$

And finally:

$$C_{tip}^{base} \approx J(q) C_q J(q)^T \tag{B.10}$$

Appendix C
Representing Tolerances

This section contains further details about the formulation for tolerances developed in Section 3.2.

C.1 Generic Formulation

A generic tolerance in 6 degrees of freedom may be represented as follows:

$$m = \sqrt{\delta X^T \mathcal{T} \delta X} \leq 1 \tag{C.1}$$

$\mathcal{T}$ is a 6×6 symmetric matrix, which encodes the tolerance requirement. The value m is a continuous, scalar measure of the displacement with respect to the tolerance. The smaller the value of m is, the less deviation there is from the nominal position. An optimisation procedure can be employed to minimise m, thus establishing the best possible performance, with respect to the necessary tolerances.

It is often convenient to consider m^2 instead of m. Note that both can be used for optimisation, since the following holds:

$$m_1 > m_2 \iff m_1^2 > m_2^2 \tag{C.2}$$

Also note that the radicand of Equation C.1 is always positive, thus $m^2 = \delta X^T \mathcal{T} \delta X$.

C.2 Combining Tolerances

Multiple tolerances can be combined to form a single tolerance. This follows from:

$$\text{If} \qquad \mathcal{T}_{\text{combined}} = \mathcal{T}_1 + \mathcal{T}_2 \tag{C.3}$$

$$\text{Then} \qquad \delta X^T \mathcal{T}_1 \delta X + \delta X^T \mathcal{T}_2 \delta X = \delta X^T \left(\mathcal{T}_1 + \mathcal{T}_2\right) \delta X \tag{C.4}$$

$$\therefore m_{\text{combined}}^2 = m_1^2 + m_2^2 \tag{C.5}$$

It is known that:

$$m_{\text{combined}}^2 \geq 0 \tag{C.6}$$

$$m_1^2 \geq 0 \tag{C.7}$$

$$m_2^2 \geq 0 \tag{C.8}$$

$$m_{\text{combined}}^2 = m_1^2 + m_2^2 \tag{C.9}$$

Thus:

$$m_{\text{combined}}^2 \leq 1 \implies (m_1^2 \leq 1) \wedge (m_2^2 \leq 1) \tag{C.10}$$

Note that converse does not hold:

$$m_{\text{combined}}^2 \leq 1 \;\not\Longleftarrow\; (m_1^2 \leq 1) \wedge (m_2^2 \leq 1) \tag{C.11}$$

This means that the combined tolerance is more restrictive than a union of the individual tolerances. This effect can be seen in Figure 3.2: the combined tolerance does not completely cover the union of the two component tolerances.

C.3 Full Drilling Example

The example of 2D drilling (Section 3.2.2) may be expanded to 3D. The tip of the drill may not displace laterally by more than ϵ:

$$\delta x^2 + \delta y^2 \leq \epsilon^2 \tag{C.12}$$

Or in matrix form:

$$\begin{bmatrix} \delta x & \delta y & \delta\theta_x & \delta\theta_y \end{bmatrix} \begin{bmatrix} 1 & 0 & 0 & 0 \\ 0 & 1 & 0 & 0 \\ 0 & 0 & 0 & 0 \\ 0 & 0 & 0 & 0 \end{bmatrix} \begin{bmatrix} \delta x \\ \delta y \\ \delta\theta_x \\ \delta\theta_y \end{bmatrix} \leq \epsilon^2 \tag{C.13}$$

The same is true for some point a distance l up the drill bit. This introduces terms for the rotation around the tip:

$$\left(\delta x + l\delta\theta_y\right)^2 + \left(\delta y - l\delta\theta_x\right)^2 \leq \epsilon^2 \tag{C.14}$$

Or in matrix form:

$$\begin{bmatrix} \delta x & \delta y & \delta\theta_x & \delta\theta_y \end{bmatrix} \begin{bmatrix} 1 & 0 & 0 & l \\ 0 & 1 & -l & 0 \\ 0 & -l & l^2 & 0 \\ l & 0 & 0 & l^2 \end{bmatrix} \begin{bmatrix} \delta x \\ \delta y \\ \delta\theta_x \\ \delta\theta_y \end{bmatrix} \leq \epsilon^2 \tag{C.15}$$

These can be combined in matrix form as:

$$\begin{bmatrix} \delta x & \delta y & \delta\theta_x & \delta\theta_y \end{bmatrix} \begin{bmatrix} 2 & 0 & 0 & l \\ 0 & 2 & -l & 0 \\ 0 & -l & l^2 & 0 \\ l & 0 & 0 & l^2 \end{bmatrix} \begin{bmatrix} \delta x \\ \delta y \\ \delta\theta_x \\ \delta\theta_y \end{bmatrix} \leq \epsilon^2 \tag{C.16}$$

The final tolerance matrix $\mathcal{T}$ is:

$$\mathcal{T} = \begin{bmatrix} \frac{2}{\epsilon^2} & 0 & 0 & 0 & \frac{l}{\epsilon^2} & 0 \\ 0 & \frac{2}{\epsilon^2} & 0 & \frac{-l}{\epsilon^2} & 0 & 0 \\ 0 & 0 & 0 & 0 & 0 & 0 \\ 0 & \frac{-l}{\epsilon^2} & 0 & \frac{l^2}{\epsilon^2} & 0 & 0 \\ \frac{l}{\epsilon^2} & 0 & 0 & 0 & \frac{l^2}{\epsilon^2} & 0 \\ 0 & 0 & 0 & 0 & 0 & 0 \end{bmatrix} \tag{C.17}$$

Note the additional rows and columns for the vertical displacement δz and the axial rotation θ_z, both of which are not penalised.

C.4 Transforming Tolerances

Much like wrenches and twists (Appendix A), tolerances may be transformed between reference and application frames.

$$m^2 = \left(\delta X_A^C\right)^T \mathcal{T}_A^C \left(\delta X_A^C\right) \tag{C.18}$$

$$m^2 = \left(\delta X_B^D\right)^T \mathcal{T}_A^C \left(\delta X_A^C\right) \tag{C.19}$$

$$m^2 = \left({}_x\mathcal{H}_{BA}^{DC} \delta X_A^C\right)^T \mathcal{T}_B^D \left({}_x\mathcal{H}_{BA}^{DC} \delta X_A^C\right) \tag{C.20}$$

$$m^2 = \left(\delta X_A^C\right)^T \left({}_x\mathcal{H}_{BA}^{DC}\right)^T \mathcal{T}_B^D \left({}_x\mathcal{H}_{BA}^{DC}\right) \left(\delta X_A^C\right) \tag{C.21}$$

Thus, a tolerance transforms as follows:

$$\mathcal{T}_A^C = \left({}_x\mathcal{H}_{BA}^{DC}\right)^T \mathcal{T}_B^D \left({}_x\mathcal{H}_{BA}^{DC}\right) \tag{C.22}$$

$$\mathcal{T}_A^C = \left({}_w\mathcal{H}_{AB}^{CD}\right) \mathcal{T}_B^D \left({}_x\mathcal{H}_{BA}^{DC}\right) \tag{C.23}$$

C.5 Uncertain Input

If the deflection is uncertain, and can be represented as a multivariate gaussian $\widetilde{\delta X}$, then the metric $\widetilde{m^2}$ is a generalised chi-squared distribution.

Two useful means of condensing the uncertain metric into a single value exist.

C.5.1 Cumulative Distribution Function

By computing the cumulative distribution function of the uncertain metric for 1, the probability that the resulting displacement is within (or at) tolerance can be found. If this CDF value is 100%, then the displacement is certainly within tolerance.

$$\mathrm{CDF}_{\widetilde{m^2}}(1) = P\left(\widetilde{m^2} \leq 1\right) \tag{C.24}$$

There is no closed form solution for the CDF of a generalised chi-squared distribution [39], however reliable numerical solutions exist, such as the algorithm described in [40].

C.5.2 Expected Value

A more computationally efficient solution is to merely compute the expected value of the metric. It can be represented as:

$$\mathbb{E}\left[\widetilde{m^2}\right] = \mathrm{tr}\left(\mathcal{T}\Sigma_{\delta X}\right) + \mu_{\delta X}^T \mathcal{T} \mu_{\delta X} \tag{C.25}$$

Note that this alone is not sufficient to indicate that the deflection is necessarily within tolerance.

Appendix D
Joint Stiffness Behaviour Plots

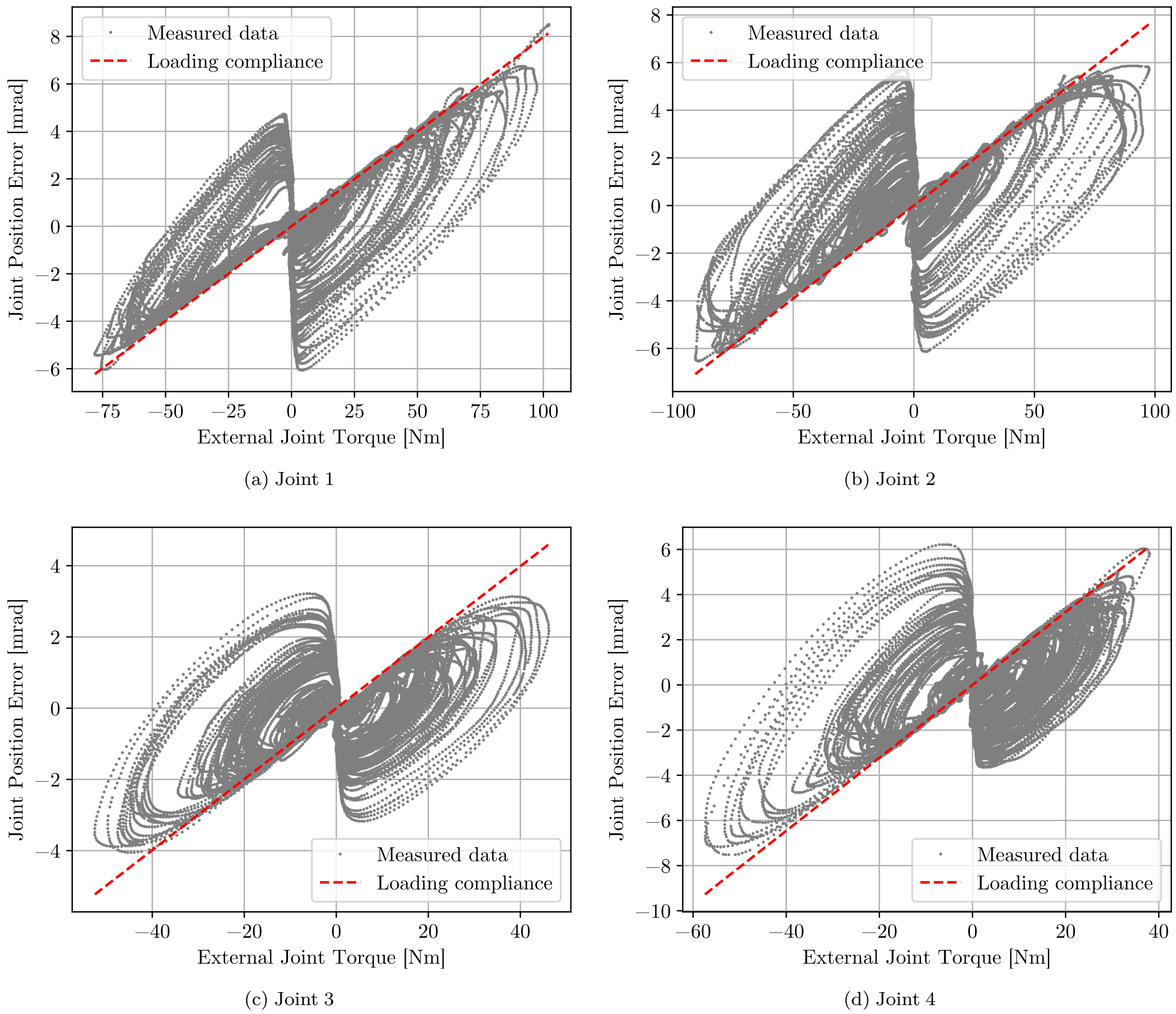

Fig. D.1: Joint position error vs external joint torque for all joints (part 1)

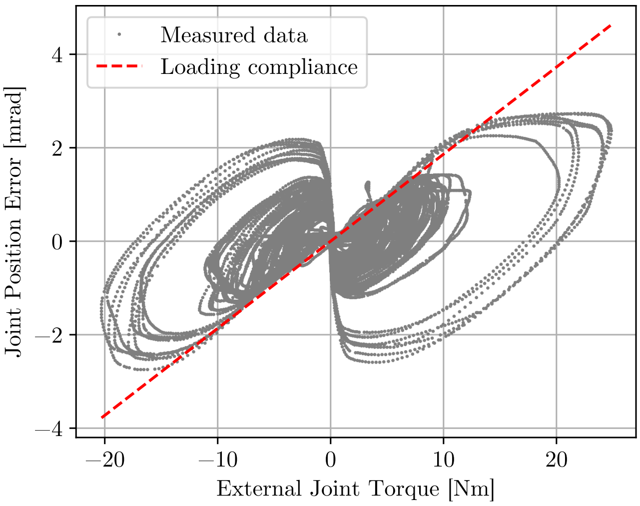

(a) Joint 5

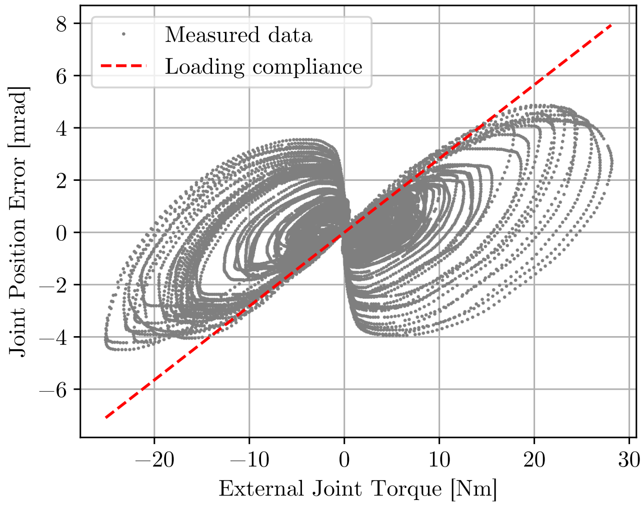

(b) Joint 6

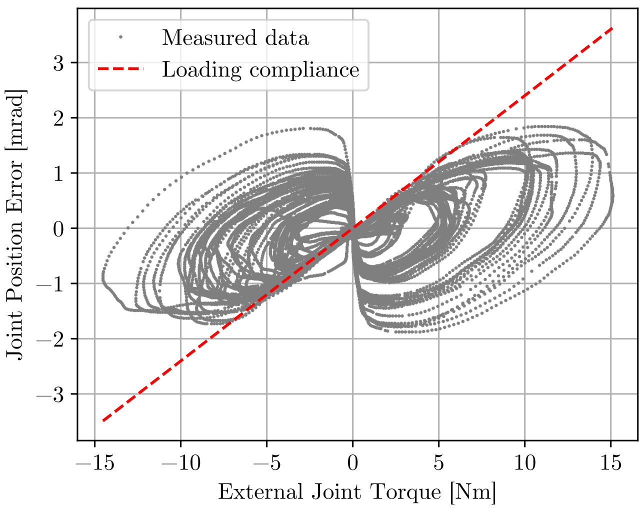

(c) Joint 7

Fig. D.2: Joint position error vs external joint torque for all joints (part 2)

Appendix E
Joint Configuration Selection

Joint configurations were semi-randomly selected, so as to produce a wide spread in tolerance stiffness metric values. Samples were taken at three viable vice orientations, and different positions of the vice. For some vice positions, multiple IK solutions could be used, however for some positions, only limited variance in stiffness could be achieved, or collisions or joint limits prevented planning for drilling at some IK seed states. To aid in selection the *reach* tool was used to find maxima and minima of the stiffness metric for different vice positions. The results of the *reach* studies are shown in Figure E.1. The grey circle is the base of the robot. Any black points indicate unreachable poses. Note that all possible vice positions are shown. In some cases these overhang over the edge of the table (grey rectangle) due to the vice mounting.

All utilised seed joint-configurations are shown in Figure E.2. The workpiece position, sample number and tolerance stiffness metric are shown for each pose (for the centre hole). Note that each sample number corresponds to a different joint configuration, but some workpiece positions are repeated. The stiffness metric values for all metrics is shown in Table E.1 (see Appendix F for plots). Note that the table shows mean values over all 5 holes, where the poses shown in Figure E.2 are for the centre hole, leading to occasional minor discrepancies in value. Also note that samples were randomly drawn from a set of 22 numbered blanks, thus some sample numbers are unused.

TABLE E.1: Stiffness metric values for all selected joint state configurations (mean over all 5 holes)
(sorted from stiffest to most compliant)

Workpiece position	**Sample Number**	**Tolerance Metric** [1]	**Axial Compliance** [$\mu m\,N^{-1}$]	**Translational Isometry** [1]	**Distance to Workpiece** [m]
88	19	0.072	39	1.7	0.46
245	11	0.079	27	1.7	0.48
85	9	0.089	37	1.6	0.46
521	2	0.21	31	3.9	0.70
85	15	0.39	44	1.9	0.46
88	8	0.71	41	1.8	0.46
506	7	1.4	67	14	0.79
555	12	3.4	74	14	0.85
555	6	4.3	77	8.4	0.85
555	4	6.0	84	20.	0.85
521	17	7.6	61	12	0.70
506	21	7.8	93	15	0.79
569	13	9.6	59	29	0.94
594	18	11	64	160	1.04

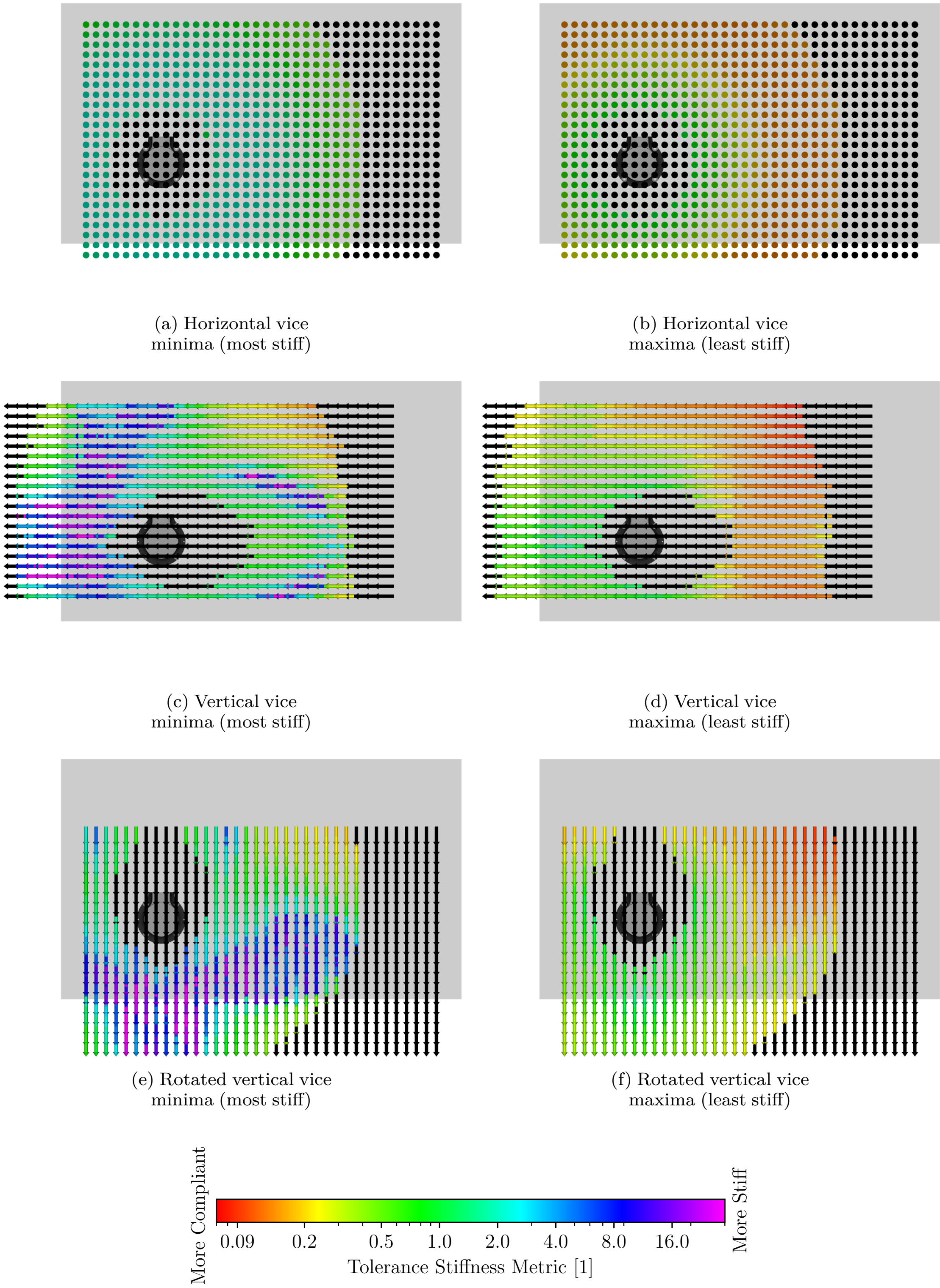

(a) Horizontal vice minima (most stiff)

(b) Horizontal vice maxima (least stiff)

(c) Vertical vice minima (most stiff)

(d) Vertical vice maxima (least stiff)

(e) Rotated vertical vice minima (most stiff)

(f) Rotated vertical vice maxima (least stiff)

(g) Legend

Fig. E.1: Top view showing stiffness metric extrema for different vice orientations and positions

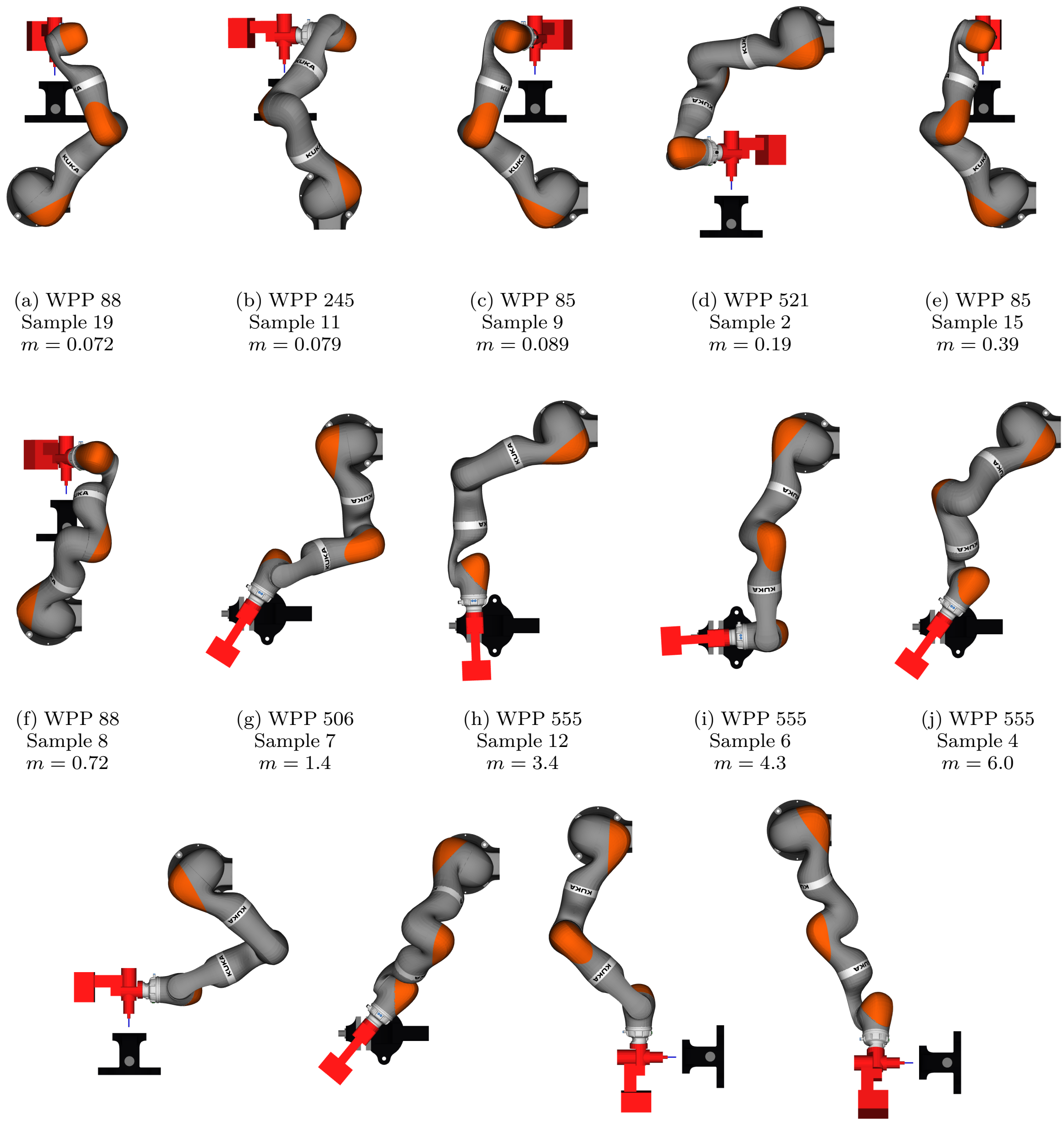

(a) WPP 88
Sample 19
$m = 0.072$

(b) WPP 245
Sample 11
$m = 0.079$

(c) WPP 85
Sample 9
$m = 0.089$

(d) WPP 521
Sample 2
$m = 0.19$

(e) WPP 85
Sample 15
$m = 0.39$

(f) WPP 88
Sample 8
$m = 0.72$

(g) WPP 506
Sample 7
$m = 1.4$

(h) WPP 555
Sample 12
$m = 3.4$

(i) WPP 555
Sample 6
$m = 4.3$

(j) WPP 555
Sample 4
$m = 6.0$

(k) WPP 521
Sample 17
$m = 7.6$

(l) WPP 506
Sample 21
$m = 7.8$

(m) WPP 569
Sample 13
$m = 9.6$

(n) WPP 594
Sample 18
$m = 11$

Fig. E.2: All joint configurations used for drilling
(sorted by tolerance stiffness metric, from stiffest to most compliant)

Appendix F
Performance Measure Correlation Plots

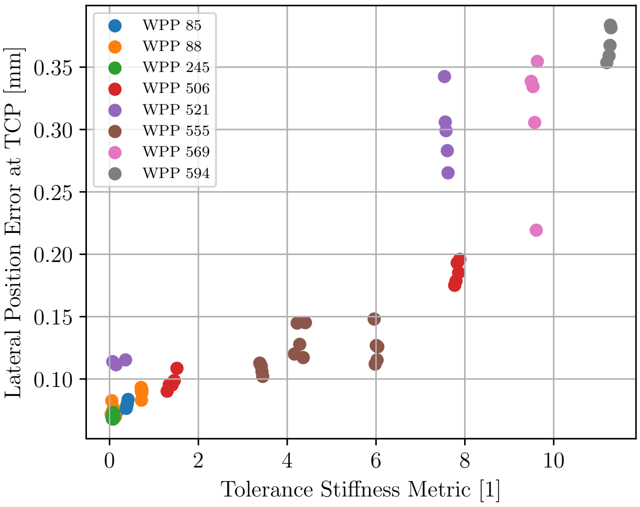

(a) Tolerance metric vs lateral controller error

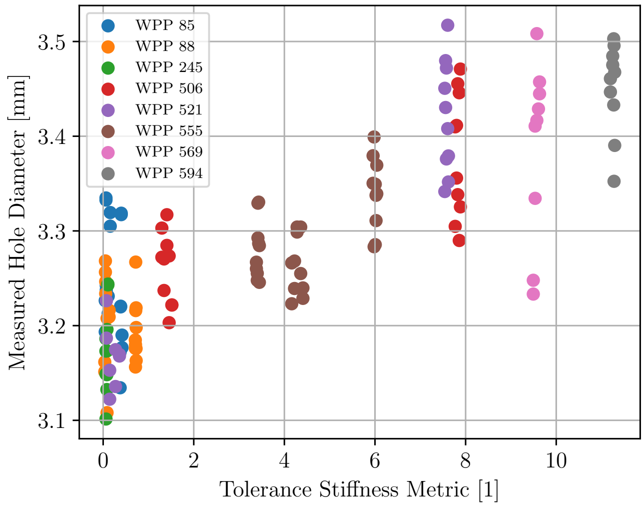

(b) Tolerance metric vs hole diameter

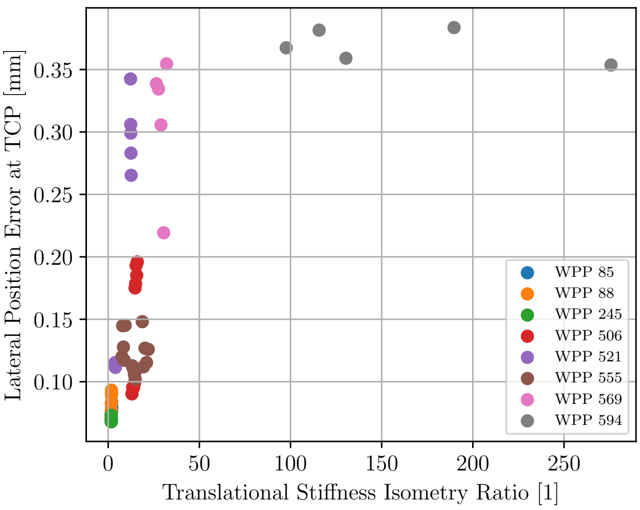

(c) Isometry metric vs lateral controller error

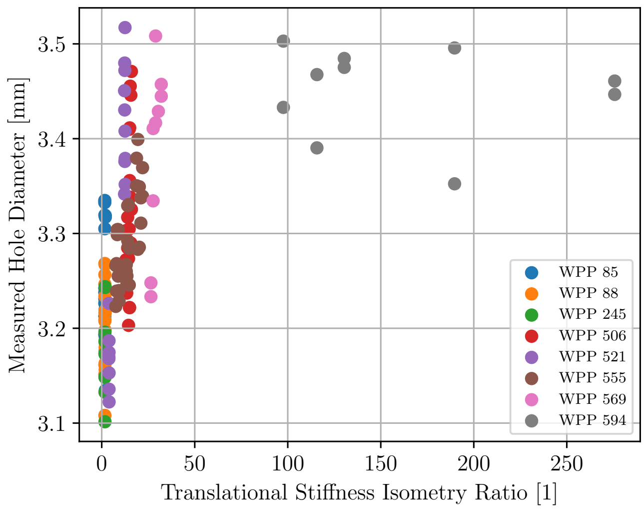

(d) Isometry metric vs hole diameter

Fig. F.1: Various stiffness metrics vs measures of process performance (part 1)
(grouped by workpiece position (WPP))

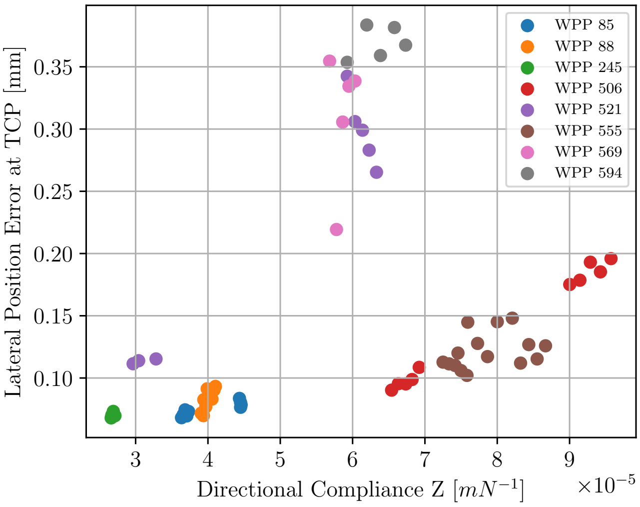

(a) Axial stiffness metric vs lateral controller error

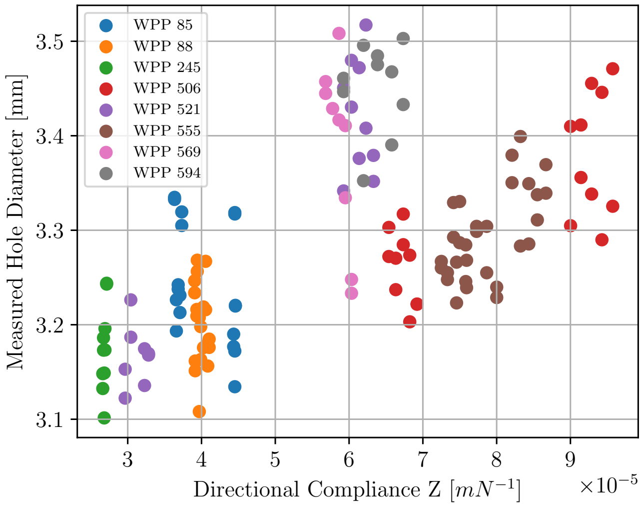

(b) Axial stiffness metric vs hole diameter

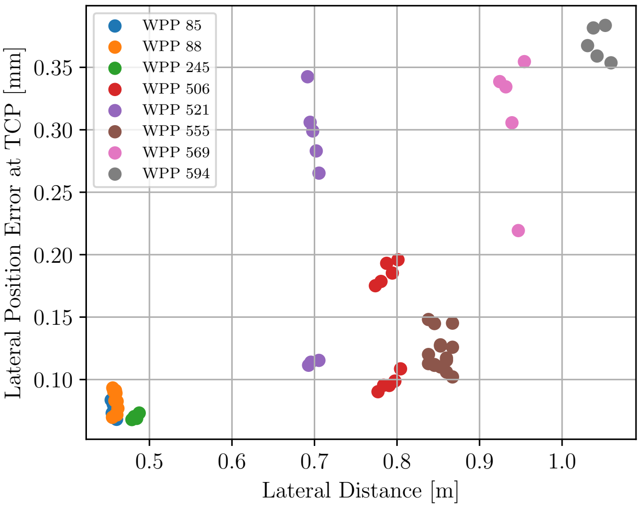

(c) Distance from base vs lateral controller error

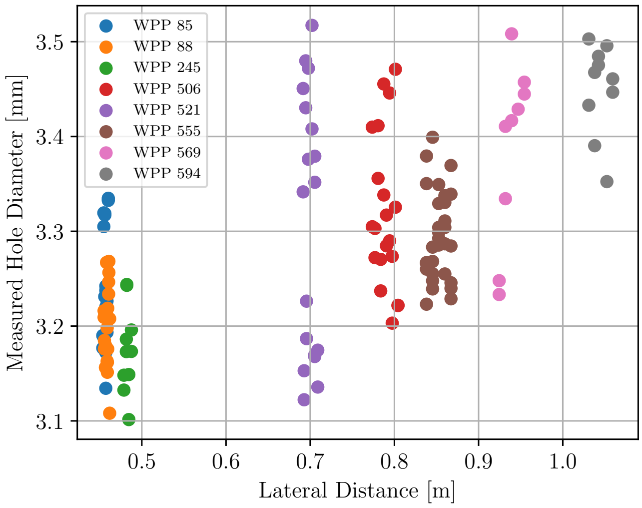

(d) Distance from base vs hole diameter

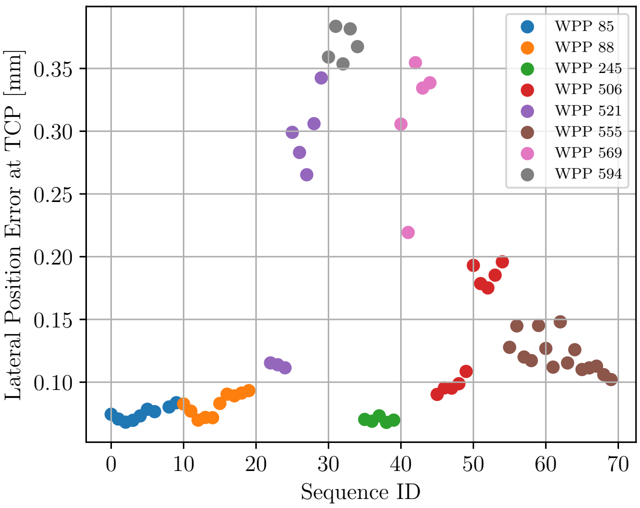

(e) Drilling sequence number vs lateral controller error

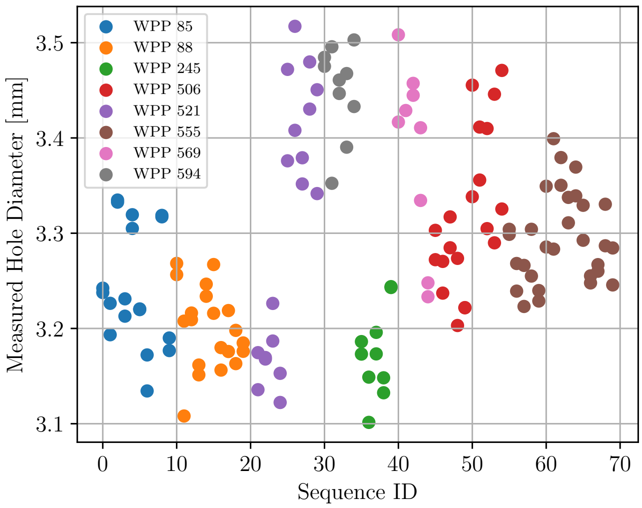

(f) Drilling sequence number vs hole diameter

Fig. F.2: More metrics vs measures of process performance (part 2)
(grouped by workpiece position (WPP))

Appendix G
Software Architecture

This section outlines how the software architecture of **reflex** was designed to retain maximum generality and flexibility.

The core is written in *C++*, using the linear algebra library *Eigen*. Implementations can build on the core functionality, to reduce the need for rewriting code when porting from one system to another. Dependency inversion [41] was employed to eliminate the need for recompiling executables when component code changes. A simplified package dependency tree is shown in Figure G.1; various utilities and minor dependencies are omitted for brevity.

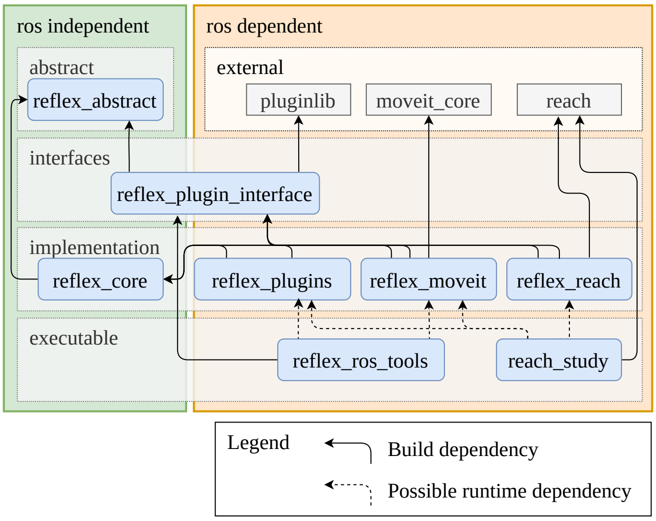

Fig. G.1: Simplified **reflex** package dependency tree

Note that the executable components only depend on the interfaces exposed by **reflex** and *reach* at runtime.

G.1 Plugin Framework

To compute the stiffness metric, three key components are needed (see Figure G.2). First, the robot stiffness model, which can be used to predict the compliance characteristics of the robot. Next, the process requirements must be formulated somehow. Finally, the stiffness metric combines the two, yielding a scalar value, the stiffness metric. These three components are loaded at runtime, allowing for simple reconfiguration without recompilation. These components are loaded from plugins.

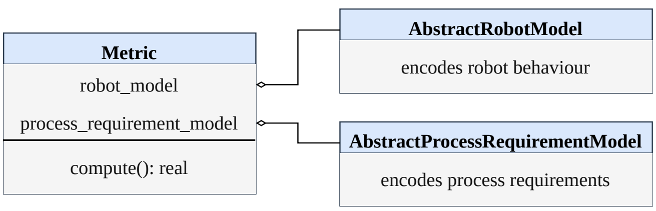

Fig. G.2: Core class structure

Upon loading, the objects are converted to the required type using dynamic casting, with checks to ensure casting succeeds.

G.1.1 Robot Model

The behaviour of the robot must be understood to perform evaluation. This includes computing the stiffness behaviour. By leveraging inheritance, complex models can be constructed from individual concepts. This leads to a hierarchy of models, which can be chosen from for metric calculations. Figure G.3 shows an overview of the currently implemented robot hierarchy. Note that it can be extended simply by writing plugins inheriting from existing models.

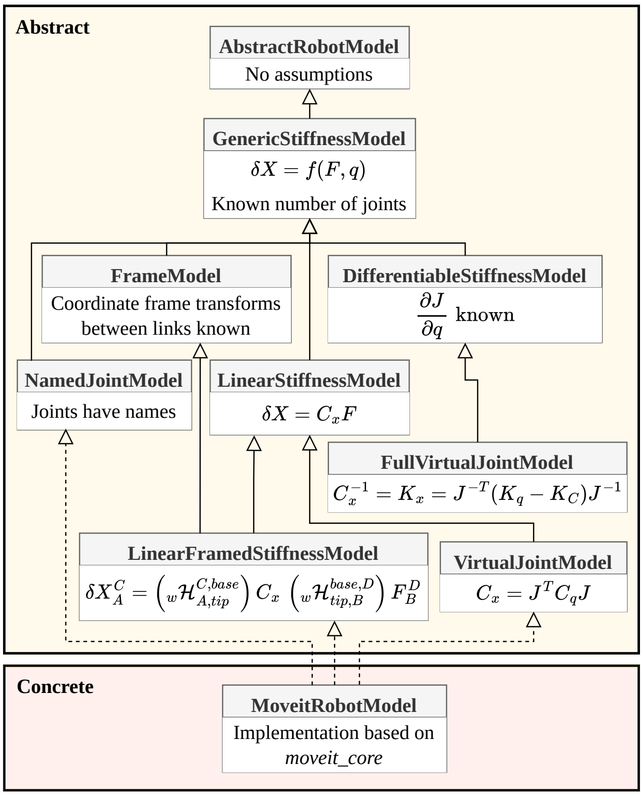

Fig. G.3: Robot model hierarchy

An instance of this plugin is implemented using *MoveIt2*, which can be used to compute the robot Jacobian and transformations between frames.

G.1.2 Process Requirement Model

Additional information external to the robot, but relevant to metric calculation is encapsulated in the process requirement model. For example, in the case of the tolerance stiffness metric, the matrix $\mathfrak{T}$ (as defined in Equation 3.11) forms part of the process requirement model.

G.1.3 Metric

Finally, a metric interface is defined. It contains a robot model and a process model. From these, it can compute the scalar metric value. Depending on the metric, specific types of robot and process models may be required. Compatibility between the runtime-loaded plugins is checked based on the requirements defined by the metric.